Degradation in photoelectrochemical devices: review with an illustrative case study

2017 J. Phys. D: Appl. Phys. 50 124002

(http://iopscience.iop.org/0022-3727/50/12/124002)

OPEN ACCESS
IOP Publishing
Journal of Physics D: Applied Physics
J. Phys. D: Appl. Phys. **50** (2017) 124002 (23pp)
doi:10.1088/1361-6463/aa5b11

Degradation in photoelectrochemical devices: review with an illustrative case study

Fredy Nandjou and Sophia Haussener

Laboratory of Renewable Energy Science and Engineering, EPFL, 1015 Lausanne, Switzerland

E-mail: sophia.haussener@epfl.ch

Received 21 October 2016, revised 12 December 2016
Accepted for publication 20 January 2017
Published 24 February 2017

Abstract

The durability, reliability, and robustness of photoelectrochemical (PEC) devices are key factors for advancing the practical large-scale implementation of cost-competitive solar fuel production. We review the known degradation mechanisms occurring in water-splitting photoelectrochemical devices. The degradation of single components is discussed in detail, and the parameters and conditions which influence it are presented. Device short-term durability depends on the semiconductor material and its interface with the electrolyte. Catalyst and electrolyte degradations are considerable challenges for long-term durability. We highlight how PEC device design choices can affect the salience of alternative degradation mechanisms. The PEC device architecture and the initial operating design point are crucial for observed device performance loss. Device degradation behavior is further impacted by irradiation intensity and concentration, and by current density and concentration. Enhancing a physical understanding of degradation phenomena and investigating their effect on component properties is of utmost importance for predicting performance loss and tackling the durability challenge of PEC devices.

Keywords: photoelectrochemistry, degradation, device modeling

(Some figures may appear in colour only in the online journal)

Abbreviations and acronyms

AFM	Atomic force microscopy
ALD	Atomic layer deposition
CB	Chemical bath
CVD	Chemical vapor deposition
ED	Electro-deposition
EDX	Energy dispersive x-ray
EL	Electrolyte
FF	Filling factor
FRR	Fluoride release rate
ICP-MS	Inductively coupled plasma mass spectroscopy
IPES	Inverse photoemission spectroscopy
PEC	Photoelectrochemical
PVD	Physical vapor deposition
RBS	Rutherford backscattering spectrometry
SC	Semiconductor
SD	Spray deposition
SECM	Scanning electrochemical microscopy
SIMS	Secondary ion mass spectrometry
STH	Solar to hydrogen
UPS	Ultraviolet photoelectron spectroscopy
XAS	X-ray absorption spectroscopy
XES	X-ray emission spectroscopy
XPS	X-ray photoelectron spectroscopy

1. Introduction

Photoelectrochemical water splitting is an attractive and clean method for the production of solar hydrogen [1]. In the future energy mix, hydrogen is considered a promising energy vector which can be produced from different renewable

energy sources, can be stored, and can be efficiently converted into electrical and/or thermal power [2–4]. Solar energy is the largest renewable energy source available, potentially capable of providing inputs greater by an order of magnitude than those required to fulfill the current primary energy demand [5].

Compared to separate photovoltaic and electrolyzer configurations, integrated photoelectrochemical (PEC) devices have the potential to increase energy conversion efficiency and to reduce hydrogen cost [6, 7]. In order for PEC approaches and devices to be of practical relevance and to have an impact in our energy economy, they must fulfill four requirements, they need to be (i) efficient, (ii) cheap, (iii) sustainable, and (iv) robust. These four demands are linked. Addressing just one or a few of them does not provide a satisfactory high impact solution.

During the last few decades, the PEC research community has focused on the development of high-performing earth abundant materials for PEC hydrogen generation [8–13]. More recently, estimations for production cost [14–17] and environmental impact [1, 18–20] have been conducted. These studies have provided a general understanding of the economic competitiveness and sustainability of PEC approaches and devices. Targets for performance and lifetime of PEC devices have usually been defined based on these cost calculations and life cycle analyses, neglecting degradation.

Globally, if one assumes that hydrogen costs in the range of \$2–\$4 per kg H_2 must be achieved in order for PEC-processed hydrogen to be competitive with steam-reformed hydrogen, efficiencies in the range of 10% and lifetimes longer than 10 years (~30 000 on-sun hours i.e. ~90 000 total operating hours) are required [15]. Instead of cost, if sustainability is prioritized and one stipulates that the device must minimally produce hydrogen with an amount of energy comparable to the energy input required to mine, manufacture, and operate the device, operational times in the range of 8 years (~25 000 on-sun hours i.e. ~75 000 total operating hours) at efficiencies above ~3% are required [18].

Including degradation in performance calculations further exacerbates this target, as indicated in a recent study by Dumortier *et al* [1], which includes component degradation at variable rates. Generally, the most durable materials for PEC devices exhibit either low efficiencies or high costs. If cost is prioritized in the application, a tradeoff between efficiency and durability is required, since the cost of a PEC device or system is roughly proportional to the ratio between the produced amount of hydrogen and the operational time. One can either increase the amount of hydrogen significantly (i.e. increase the efficiency) for a given operational time, or increase the operational time at a given production of hydrogen with a reasonable degradation rate. Both approaches reduce hydrogen cost. Dumortier *et al* [1] showed this tradeoff in a case for which they assumed that single components in a PEC device can be replaced individually. They observed two local minima in hydrogen price: one minimum for the case where the components were replaced fairly regularly, and one minimum where the components were never replaced and operated at low rates towards the end of the device lifetime. The severity of the observed cost minima, however, were dependent on the degradation rates of the various components.

In a review of PEC demonstrations, Ager *et al* [21], concluded that while efficiencies in the range of 10% or more are reasonable for PEC devices (with direct semiconductor-electrolyte junctions as well as buried junctions), stability across the complete pH range ($0 \leqslant \mathrm{pH} \leqslant 14$) proves challenging, and is seldom investigated. Most studies reviewed by Ager *et al* [21] were limited to an operational demonstration for less than 24 h. Ager *et al* concluded that device stability, durability, reliability, and robustness are the major challenges for PEC commercialization. *Stability* is the ability of a PEC device to perform within a narrowly defined performance window during continuous operation and over a short timescale. *Durability* is considered the ability of a PEC device to maintain its performance and product purity over the lifetime, i.e. withstanding non reversible degradation and punctual failures. *Reliability* is the ability of the PEC device to perform above a specified level for a certain period of time, while avoiding catastrophic failure. From a practical standpoint, this involves statistical probabilities, assessing reliability as the mean time between failures. *Robustness* is the ability of a PEC device to tolerate various imperfections and stress factors without exhibiting dramatic failure.

We define the *lifetime* of a device as the shorter operational time of the two: (i) the operational time during which a device either operates above a well-defined performance threshold (i.e. durable), or (ii) the operational time during which a device operates without sudden, catastrophic failure (i.e. reliable). It is worth noting that there are significant uncertainties in the definition of the lifetime of PEC devices cited in literature. This is related to the fact that there are neither the reference test conditions, nor end of life criteria needed for a rational comparison of different devices [22, 23].

Reference conditions for PEC lifetime benchmarking could draw inspiration from the photovoltaic and fuel cell/electrolyzer research communities. In the photovoltaic research community, the lifetime target for solar modules is around 80 000 on-sun hours (i.e. 25 years) with an end of life defined as 20% loss in efficiency [24]. In the fuel cell and electrolyzer research communities, the lifetime target for water electrolyzers for hydrogen production is around 80 000 h (i.e. ~ 9 years) in stationary conditions, with less than a 10% loss in performance at the end of life [25]. Note that for PEC devices, the intermittency of solar radiation might exacerbate performance loss [26]. In order to consider intermittency, accelerated testing conditions which mimic lifetime exposure to varying operational conditions can be established [27–30].

Significantly different lifetimes and operational times of PEC device demonstrations have been reported (differing by orders of magnitude) in literature [21, 31–33]. During long-term operation, all demonstrations showed diminished performance, and some failed catastrophically. Generally, it has been observed that higher durability is obtained for devices consisting of semiconductors which are isolated and protected from the electrolyte (buried PV). Indeed, the most efficient semiconductors for solar fuel production, such as Si, GaAs, GaP, are prone to corrosion in aqueous solution [34].

Table 1. Semiconductor, anodic, cathodic, and overall reactions occurring in a water-splitting PEC device in acidic, base, or neutral conditions.

	Acidic	Basic
Semiconductor	$4h\nu \rightarrow 4e^- + 4h^+$	
Anode	$2H_2O + 4h^+ \rightarrow O_2 + 4H^+$	$4h^+ + 4OH^- \rightarrow O_2 + 2H_2O$
Cathode	$4e^- + 4H^+ \rightarrow 2H_2$	$4H_2O + 4e^- \rightarrow 4OH^- + 2H_2$
Overall	$4h\nu + 2H_2O \rightarrow 2H_2 + O_2$	

Commercial semiconductors such as Si are prone to oxidation in aqueous media and develops a SiO_2 passivation layer, reducing performance [35]. Semiconductors are therefore typically passivated with corrosion resistant and conductive films, which, ideally, are also optically transparent when used on the top of the photoabsorber.

For devices using high performing semiconductor-liquid junctions, few cases showed stabilities longer than 1 d while also ensuring continuous high efficiencies [36–41]. The longest operational demonstration is about 2200 h [42]. Metal oxide-based photoabsorbers are more stable but generally exhibit lower efficiency due to inherent limitations in the bulk transport. Hematite (α-Fe_2O_3) and bismuth vanadate ($BiVO_4$) are two photoabsorber examples which show considerable stability with efficiencies close to their (low) theoretical maximum [43]. Besides the stability of the semiconductor, degradations of the co-catalyst and electrolyte also impact performance [44, 45]. The high acidity or basicity, high humidity, and high potential of the operating environment can drastically affect catalyst stability, while operating temperature and pressure highly impact electrolyte degradation [26, 46, 47].

Generally, device architecture and operation significantly affect performance loss through different degradation mechanisms and typical degradation rates participating in the destruction of the device. Different interfaces are prone to different degradation mechanisms depending on design. Design as well as device operation furthermore affect spatial inhomogeneity of the various property fields such as: current densities, temperature, or the species concentrations at the interfaces and in the semiconductor, catalyst, or electrolyte components. These spatial heterogeneities and the corresponding gradients induce and intensify degradation mechanisms [48].

Real-time transients in solar irradiation also significantly affect degradation behavior [26]. Transients include three time-scales: short-time transients (seconds) due to clouds passing, medium-time transients (hours) due to diurnal solar movement, and long-term transients (months) due to seasonal variation in irradiation. Short-term transients induce large temporal temperature gradients and short-term accumulation of charge which can negatively affect performance [49, 50]. Medium-term transients allow for back and competing reactions in the dark, potentially reversing some of the degradation effects as well as introducing additional 'dark' degradation mechanisms [51]. Long-term gradients mostly affect the irradiation magnitude incident on the device, which can be much larger in the summer than in the winter. Consequently, degradation mechanisms which are mostly driven by the magnitude of photon flux might be more relevant in summer than in winter. Moreover, start and stops as well as freeze and thaw cycles can induce transitory effects which severely amplify degradation mechanisms [52–54].

As known from the fuel cell community, it is additionally important to differentiate between single device and stacked device performance. Even for a very durable laboratory scale fuel cell, it has been observed that a large area stack performs with limited durability [55, 56]. Such considerations become particularly important when thinking about the scaling of a device into a commercial system. At this point, it is quite unclear what the scaling of PEC devices should look like. Stacking is limited to directions which do not require direct irradiation, potentially reducing the density of the devices and their ability to influence each other's performance.

As the maximum achieved length of operational demonstrations (~2000 on-sun hours) are far from commercially relevant operational times (~30 000 on-sun hours), research efforts must concentrate on an understanding of degradation mechanisms occurring in devices and at component interfaces, as well as the impact of these mechanisms on performance. Furthermore, understanding how device design and operational choices affect the salience and magnitude of alternative degradation mechanisms has the potential to provide guidance for the best likely design scenarios. Here, we review and discuss the different degradation mechanisms that occur in PEC devices together with how device architecture and operation can influence degradation. After a brief introduction of PEC device components, materials, and interfaces in section 2, we present a comprehensive review of the different degradation mechanisms reported in literature and discuss the impact of reported degradation mechanisms on performance. In the final section, we present an illustrative case study in order to provide insight into the complex interplay between design, operation, degradation, and operational time-dependent performance.

2. Operating principle, materials, and designs

The functional steps taking place in a photoelectrochemical device are (i) photoabsorption in the semiconductor, (ii) charge generation, separation and transport towards the interfaces, (iii) catalytic electrochemical reactions, (iv) ionic transport through the electrolyte, and (v) product separation and collection. Photon energy ($h\nu$) is converted into an electron–hole pair in the semiconductor if the band gap energy of the material allows it[1]. The electrons and holes are separated by an electric field and diffusion gradients, and are transported to an

[1] We do not discuss novel concepts which include upconversion, hot carriers, or similar.

interface sometimes covered with additional electrocatalyst. Then, they are transferred across the semiconductor-electrolyte or catalyst-electrolyte interface in order to drive electrochemical reactions. The catalyst is used to increase the rate of redox reactions and enhance selectivity towards a particular reaction. An electrolyte connects the anodic and cathodic reaction sites in order to close the electrical circuit. This closure is obtained through the transport of the produced ions (H^+ or OH^- depending on the electrolyte). The simple one-step electrochemical reactions which take place in a water-splitting device in acid or basic conditions are given in table 1.

In the simplest case, a PEC device consists of a photocatalyst and an electrolyte only. More frequently, the functionality of the photocatalyst is decoupled and distributed towards additional subcomponents: multiple semiconductors, co-catalysts, and conduction layers. Overall PEC device functionality is further enhanced by introducing protection and interface layers, and product separators. We focus here on PEC devices which include a photoabsorber (semiconductor), additional electrocatalysts, and an electrolyte.

2.1. Semiconductor

The semiconductor's functions include photon absorption, and charge generation, separation, and transport. Absorption is related to its band gap and its imaginary part of the refractive index. The band gap must be large enough to drive the electrochemical reaction, which includes an equilibrium potential (1.23 V at standard conditions) and different additional overpotentials due to catalyst activation, ohmic losses, and mass transport limitations. The refractive index provides information on semiconductor thickness, which is required for photon absorption. The transport of the generated charge carriers is characterized by their mobility and lifetime (both of them are coupled to the diffusion length). The separation of the carriers depends on the design of the system, and on the transport properties and doping concentrations of the semiconductor. A tradeoff between typical absorption length and typical carrier diffusion length is needed to ensure effective charge separation.

There are two main categories of semiconductors:

- *Non-oxide semiconductors*. In this category, we can list, for instance, single elements of group IV (Si, Ge), and compounds of group III–V and II–VI (GaAs, GaP, InP, CdS, CdTe, etc). These exhibit high efficiencies, as they have been researched for decades in the photovoltaic community. Their disadvantages are their cost, low scalability, and the amount of energy required for their production [57]. In order to increase their performance, different types of non-oxide semiconductors can be assembled in tandem devices (n-GaP/p-GaP, p-CdTe/n-TiO_2, p-CdTe/n-$SrTiO_3$, p-GaP/n-$SrTiO_3$, etc). However, non-oxide semiconductors lack stability when embedded in liquid solutions.
- *Metal oxides and oxynitrides* (Fe_2O_3, $BiVO_4$, WO_3, TiO_2, SnO_2, Cu_2O, TaON, etc). These have the advantage of good stability in aqueous solutions [58], but their wide band gap and poor electronic properties limit device performance [43, 59].

The degradation of a semiconductor can induce a change of its bulk properties and affect photon absorption behavior (i.e. affect band gap as well as the refractive index), and its ability to generate charge carriers, and separate and transport them (i.e. affects mobilities, lifetimes, recombination rates and similar). Degradation can furthermore affect the surface properties of the semiconductor (which can additionally induce changes in the bulk properties). The chemical resistance at the interface with the liquid electrolyte is essential for a durable device. For this reason, in some PEC devices [32], the semiconductor is directly protected by a coating or physically separated from the aqueous environment.

2.2. Electrolyte

The electrolyte ensures ionic transport (H^+ or OH^-) between the anode and cathode, and separation of the products (hydrogen and oxygen). The electrolyte can be liquid or solid and must be able to contain the photoabsorber and catalyst. Typical liquid electrolytes are H_2SO_4, KOH, and NaOH. Given that the ionic transport is coupled to mass transport in the fluid, liquid electrolytes are usually strongly acidic or basic in order to reduce the ionic transport resistance and the Nernstian potential losses due to pH gradients. The side effect of such a choice is an aggressive environment for the semiconductor and catalyst. Besides the ion transport, liquid electrolytes also provide a reactant (water) and ensure product removal (especially in a flow design). For solid electrolytes, the functions of the electrolyte and the reactant supply are separated, and additional flow delivery and removal components are required (e.g. flow field plates). Additionally, solid electrolytes often allow semi-permeability for gaseous products, providing separation functionality.

Polymer membranes like perfluorosulfonic acid, sulfonated polyether ketones (S-PEEK), polyether sulfones (PES), and poly benzimidazoles (PBI) are the most widely used solid acid electrolytes [60–62]. Other promising materials include hydrocarbon-based membranes [63], composite materials [64, 65] and radiation-grafted membranes [66, 67]. The most mature technology is Nafion®, a perfluorosulfonic acid membrane [68]. It not only has a relatively high proton conductivity and low gas crossover, it also has reasonable mechanical, chemical, and thermal stability.

Alkaline diaphragms can be composed of silicate materials (e.g. asbestos) [69, 70], polymer materials (e.g. PES) [71, 72], metal oxides (e.g. nickel oxide) [73] or composite materials (e.g. Zirfon®) [70, 72]. Compared to solid acid electrolytes, alkaline diaphragms generally have lower ionic conductivities, slower dynamics, and higher gas crossover. However their main advantage is higher durability and robustness.

Degradation observed in solid electrolytes is related to chemical attacks, hygrothermal stresses due to changes in temperature and humidity, and mechanical stresses due to pressure gradients between the anode and the cathode compartments. Reinforcement (e.g. TiO_2) is often used to ensure

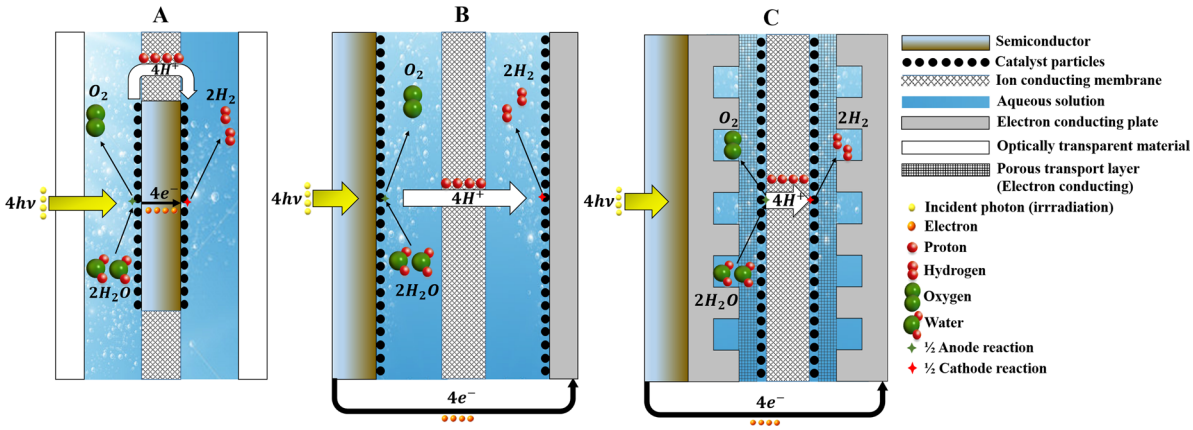

Figure 1. Different photoelectrochemical device designs. Design A: monolithic design, in which the catalyst-covered semiconductor is completely immersed in the liquid electrolyte. The catalysts, the semiconductor, and the electrolyte/separator are directly exposed to irradiation. Design B: wired design, with two separated electrodes in a liquid electrolyte. The catalyst-covered photoabsorber and counter electrode are directly exposed to the liquid electrolyte. Only the photoabsorber is exposed to direct irradiation. Design C: wired design with a separated membrane-electrode assembly, operating in the dark. The photoabsorber is not in direct contact with the electrolyte.

mechanical resistance. The generation of gaseous products at the triple phase boundary (between catalyst, solid electrolyte, and liquid reactant), and the transport of nearly saturated or supersaturated products, may induce additional mechanical stresses and delamination of solid electrolytes. The durability of the solid electrolyte or separator is crucial for PEC device reliability and safety because cracking or perforation leads to a direct recombination of the produced hydrogen and oxygen, as well as a potential buildup of explosive mixtures.

The main degradation mechanisms observed in liquid electrolytes are related to their contamination by impurities, decomposition of their components, and the accumulation of gas bubbles [69, 74], all of which affect ion transport and the purity of produced hydrogen.

2.3. Electrocatalyst

The development of earth-abundant, efficient, and stable electrocatalysts remains a great challenge [75]. The electrocatalyst supports the catalytic reaction and provides selectivity towards a certain reaction product. It should reduce the activation overpotential of the redox reactions by enhancing the kinetics of charge transfer across the interface, and by avoiding the accumulation of charge carriers at the electrode surface. Electrocatalysts (termed co-catalysts) are often deposited directly on the photoabsorber, either as thin layers or as nanoparticles. The synthesis technique considerably impacts the efficiency and stability of the catalyst [76, 77]. Catalysts can be pure active metals (Pt, Pd, Ni, etc), mixed metals (NiCo, NiMo, NiMoFe, etc), or active metal oxides (RuO_2, IrO_2, SrNbO, etc).

At the cathode, the catalyst can be carbon-supported (in powder form or as nanotubes) or self-supported. At the anode, the high potential and oxygen concentration requires that carbon supports are avoided because of corrosion. Moreover, the operating environment of acidic electrolyzers implies the use of distinct materials (noble catalysts). The addition of a proton conducting material (e.g. solid electrolytes made of ionomers) can improve the proton conduction from the catalyst particles to the electrolyte, reducing both charge accumulation and potential side reactions, as well as the stability of catalyst particles, as it acts like a binder [46]. However, direct exposure of catalyst particles to solid electrolyte, sometimes highly acidic in nature (e.g. Nafion®), leads to catalyst corrosion.

2.4. Reference designs

The three components presented above (semiconductor, catalyst, and electrolyte/separator) can be arranged in three reference designs (figure 1). These PEC device designs use planar photoelectrodes. There are other configurations in term of geometry, dimensions, and orientation [45, 78–82], but we have identified these three designs as representative of the various interfaces which can exist between the different components and the surrounding environment. These designs are prone to different degradation phenomena.

Design A is a monolithic design (wireless) in which the catalyst-covered semiconductor is completely immersed in the liquid electrolyte [83, 84]. The catalyst is directly exposed to irradiation and therefore photocorrodes. There is lateral and transversal ion transport in the cell, which generally induces larger ionic resistances [78] and larger current density heterogeneities. The latter can induce heterogeneous degradations of the components over the active area. All three components (semiconductor, solid electrolyte/separator and catalyst) are potentially in direct contact with liquid electrolyte on both sides and therefore can be chemically attacked. The catalyst can (i) be applied in a pattern (e.g. as nanoparticles), partially exposing the photoabsorber to the electrolyte, or (ii) conformably cover the photoabsorber, mitigating the direct photoabsorber-electrolyte interface and acting as a protection layer. However, in the latter case the catalyst needs to be sufficiently thin or optically transparent to ensure that enough light effectively reaches the photoabsorber. In a wireless design, device diagnostics and characterization is difficult, as the current

cannot be directly measured because a connection to external wires, which are often prone to chemical degradation, is not present. Instead, the experimenter is limited to analyzing gaseous products (through gas chromatography, mass spectrometry) and liquid concentrations. The solid electrolyte or separators can be a polymer membrane, a thin capillary, or a porous media. The separator as well as the liquid electrolyte are directly exposed to solar irradiation.

Design B is a wired design with two separated electrodes [85, 86]. Only one side of the semiconductor is exposed to the liquid electrolyte and the other side is directly exposed to irradiation. This arrangement limits the chemical attack of the semiconductor by the electrolyte. The ion transport is perpendicular to the photoelectrode and a wire is used for electron transport between the semiconductor and the counter electrode. Ribbons are deposited on the top of the semiconductor for current collection. The corrosion of ribbons and degradation of contact between the ribbons and the semiconductor induce additional performance losses compared to Design A. The catalysts, the solid and liquid electrolyte, and the counter electrode, however, are not directly exposed to solar radiation and potentially will work under completely dark conditions, mitigating photo-driven degradation mechanisms.

Design C is a wired design utilizing a separated photoabsorber and membrane-electrode assembly [10, 87]. The electrolyte is a solid membrane sandwiched between the electrodes. A liquid electrolyte containing the reactant can additionally be used [49], however it is not required for the functionality of the device. Catalyst layers are mandatory in this case because the photoabsorption and charge generation functionalities are completely separated from the electrochemical reaction and ionic charge transport functionalities. Charge carriers are transported from the semiconductor to the electrodes using a wire and bipolar plates. The latter also supply reactive water and remove the products utilizing integrated water channels. In order to ensure good fluid and charge transport from the bipolar plates to the active sites, conductive porous transport layers are used between the bipolar plates and the catalyst layers. This design clearly separates the semiconductor and the reactive environment of the device, a potential advantage from a degradation point of view. Such a separation also allows a larger choice of semiconductor materials (those which are otherwise intrinsically not stable).

In addition, Design C is capable of taking advantage of advances in the photovoltaic and electrolyzer communities or industries. Solar cells and solid electrolyte electrolyzers are relatively mature technologies with lifetimes as high as 80 000 h for photovoltaics [88] and as high as 60 000 h for electrolyzers (in stationary operation) [89]. However, the separated design introduces additional complexity and fabrication steps related to the addition of components including: conductive porous transport layers, bipolar plates, wiring, busbar deposition, and mandatory electrocatalysts. Coincidently, projected costs will increase, and performance is expected to decrease due to the charge transport in the additional components, and due to added component degradation.

3. Component degradation

PEC degradation is largely driven by interface phenomena, where the interfaces between solid materials (especially the semiconductor) and liquid electrolyte represent the greatest challenge. This challenge is intensified by the fact that some materials with good photoabsorption behavior and interesting band alignments are inherently non-stable, and therefore degrade within hours. We dedicate the first subsection here to semiconductor-liquid electrolyte (SC-liquid EL) interfaces. The second subsection is dedicated to degradation of semiconductor bulk material. The last subsections are dedicated to degradation of the electrolyte and electrocatalyst.

3.1. Semiconductor-liquid electrolyte interface

Degradation at the semiconductor-liquid electrolyte (SC-liquid EL) interface (see Designs A and B) is a result of reversible and irreversible chemical reactions [90]. Corrosion, intercalation, and hydroxylation are the most important phenomena at the SC-liquid EL interface contributing to degradation of performance, reduction in lifetime, and reduction in durability and reliability of the PEC device.

3.1.1. Corrosion. There are three different types of corrosion in photoelectrochemical devices, depending on the reactions occurring across the solid SC-liquid EL interface: chemical, electrochemical, and photoelectrochemical. Chemical corrosion is the destruction of the semiconductor due to chemical action of the surrounding environment, without the necessity of net charge transfer across the solid-liquid interface. A fundamental requirement for the choice of the semiconductor is therefore its stability in the face of chemical corrosion. Given that the corrosion mechanism does not involve charge transfer, it can also occur in the dark, i.e. during night-time operation or to components that are shielded from irradiation. The Pourbaix diagram [91] of materials can be used to identify the pH and potential range for which the material is stable against chemical corrosion. For example, silicon is prone to chemical corrosion in alkaline media [32, 92–94].

Electrochemical and photoelectrochemical corrosion, however, require a net charge transfer between the electrolyte and the semiconductor. While electrochemical corrosion involves majority charge carriers, photoelectrochemical corrosion involves photoexcited minority charge carriers. Photoelectrochemical corrosion is the most critical issue for photovoltaic cells immersed in liquid electrolytes (a variation of Designs A and B). The global equations of anodic and cathodic decompositions of a compound semiconductor[2] MX can be written as follows [58, 95]:

$$MX + zh^+ \rightarrow M^{z+}_{(aq)} + X + \Delta G_a \quad (1)$$

$$MX + ze^- \rightarrow M + X^{z-}_{(aq)} + \Delta G_c \quad (2)$$

[2] Note that for elemental semiconductors such as Si, M and X are the same zerovalent element.

M and X are insoluble species, forming a film on the surface of the semiconductor and protecting it from further corrosion (passivation). The passivation layer is often electrically non-conductive.

The composition of the corroded layer has the potential to highly impact the photoelectrochemical response of the entire semiconductor, affecting semiconductor photoabsorption and photocatalytic behavior [96]. Some oxide layers like indium oxide are photoactive, thus, they can enhance the photocurrent. $M_{(aq)}^{z+}$ and $X_{(aq)}^{z-}$ are ions which are solvated in the electrolyte (dissolution). They can be transported out of the device or deposited on other components. Dissolution implies a continuous destruction of the semiconductor, a induces pollution of the reactive environment, and can lead to sudden device failure. ΔG_a and ΔG_c are the free energy changes related to the decomposition reactions. As an example, the anodic decomposition of GaAs in a liquid electrolyte is [51]:

$$\mathrm{GaAs} + 6h^+ + \ 2\mathrm{H_2O} \rightarrow \mathrm{Ga}_{(aq)}^{3+} + \mathrm{AsO_2^-} + 4\mathrm{H^+} + \Delta G_a \tag{3}$$

Gerischer *et al* [97] related the quasi-Fermi levels of minority carriers to the corrosion potentials in order to determine a thermodynamic stability criterion of semiconductors under illumination. The Gerischer stability criterion (equation (4)) states that there is stability at the SC-liquid EL interface if the reductive potential $E(H^+/H_2)$ is higher (more positive in potential versus NHE) than the cathodic decomposition potential of the semiconductor $E_{n,d}(\mathrm{pH})$, and if the oxidative potential $E(O_2/H_2O)$ is lower (more negative in potential versus NHE) than the anodic decomposition potential of the semiconductor $E_{p,d}(pH)$.

$$\text{Stability criterion}: \begin{cases} E_{p,d}(\mathrm{pH}) > E(\mathrm{O_2/H_2O}) \\ E_{n,d}(\mathrm{pH}) < E(\mathrm{H^+/H_2}) \end{cases} \tag{4}$$

The cathodic and anodic thermodynamic decomposition potentials $E_{n,d}$ and $E_{p,d}$, which depend on the pH of the solution, can be obtained from electrochemical experimentations or thermodynamic calculations.

Multiple studies [58, 59] have shown that all commercial non-oxide semiconductors are prone to anodic decomposition, and that only a few are resistant to cathodic decomposition. For instance, Young *et al* [40] demonstrated a maximum of 120 h stability of unmodified GaAs photocathodes at -15 mA cm^{-2} in acidic electrolyte (3 M sulfuric acid), despite inherent instability in acidic conditions. Oxide semiconductors are generally stable against cathodic photocorrosion, but only a few of them (e.g. TiO_2, $BiVO_4$, Co_3O_4) are stable against anodic photocorrosion [58].

Some materials can maintain a good photocurrent stability despite corrosion. For example, Zhou *et al* [98] demonstrated that copper vanadate is a promising photoanode, showing good stability in alkaline electrolyte despite the emergence of a self-passivating layer caused by corrosion. When this passivation layer remains below a certain critical thickness, its effect on performance is not dramatic.

Once thermodynamic conditions are assessed and a potential for semiconductor decomposition is observed, kinetic factors should be considered in order to understand how fast the material will be dissolved or passivated. Strategies to affect kinetics include the addition of suitable co-catalysts that could substantially limit the rate and selectivity of the photocorrosion reaction [99]. Moreover, the degradation of the catalyst can have the side effect of increased semiconductor photocorrosion, accelerating overall degradation. The investigation of the passivation or dissolution rate can help to predict the lifetime of a device and provide guidance for an improved device design. Certainly, there is a critical thickness of the corrosion based passivation layer, above which the performance drops due to charge transport inhibition and the increase of recombination due to vacancy defects. There is also a critical corrosion thickness (for dissolution) below which there is failure due to local destruction of the semiconductor. The evolution of the thickness of the corroded layer can be calculated using the concentration of the different reactants together with the rate constants of the reactions involved in photocorrosion. Obviously, the device design and operational conditions will influence the concentration distribution of different reactants. Rate constants need to be computed or measured to this end. Lai *et al* [100] used scanning electrochemical microscopy to investigate the kinetics of photocorrosion at the interface between an illuminated semiconductor (n-type GaAs) and an electrolyte ($Fe_2(SO_4)_3/H_2SO_4$). The rate constant was 0.5-order dependent on the concentration of Fe^{3+}, and typical rates were ~10^{-4} mol m^{-2} s^{-1}. They identified two contexts affecting the electrochemical formation of the corrosion product (passivation or dissolution): (i) at low illumination intensities, growth is limited by the charges generated and transported to the interface, and (ii) at high illumination intensities, growth is limited by mass transfer in the solution.

The application of protective films can be used to enhance durability and robustness of non-corrosion resistant semiconductors working in aggressive aqueous electrolytes [51]. Typical layer thicknesses are around a few nanometers. These layers have been shown to allow otherwise unstable PEC devices to operate for more than 1000 h with minimal reduction in efficiency [36]. The main challenge remaining is to ensure long term stability while maintaining good performance. There are two main categories of protective layers:

Metals (Pd, Pt, Ni…). Metal films need to be thermodynamically stable and sufficiently thin to be transparent to incident radiation. For photoanodes, metal films can be prone to anodization (i.e. anodic corrosion), leading to a porous structure in the film [32]. For this reason, protective films should be thicker than the anodization depth, which can be measured via x-ray photoelectron spectroscopy [101]. There is, then, a thickness tradeoff between optical transparency and protection. Pt, Ni and other metals are also good electrocatalysts for HER and/or OER, and therefore, can act as both a protection layer and co-catalyst.

Metal oxides. Three subcategories of metals oxides have been tested for semiconductor protection: (i) catalytically inactive wide band gap metal oxides (examples are TiO_2, ZnO, AL_2O_3, MgO), (ii) catalytically inactive transparent conducting oxides (indium tin oxide, fluorine-doped tin oxide, aluminum-doped zinc oxide), and

(iii) catalytically active metal oxides (Fe_2O_3, MnO_x, NiO_x, CoO_x, doped SiO_2).

Catalytically inactive wide band gap metal oxides (the first category of *Metal oxides)*, have a proven stability with reasonable performance losses [102, 103]. However, they can limit performance due to unfavorable charge transport properties. Didden *et al* [104] studied photocorrosion of TiO_2 coatings and concluded that their degradation initiated from small pinholes. The obtained corrosion current showed reproducible oscillatory peaks explained by an Avrami-type photocorrosion model [105], which proposes the following law for the fraction of materials, φ, converted into a new phase, at a certain time, t:

$$\varphi = 1 - \exp(-ct^n) \tag{5}$$

The constant c is the product of a shape factor, the effective number of nuclei, and the direction-averaged growth rate. The exponent, n, is the sum of the dimension of the crystal growth process (1 = needle-like growth, 2 = plate-like growth, and 3 = 3D growth) and an integer value describing the nucleation rate (1 = a constant nucleation rate and 0 = the absence of nucleation).

Catalytically inactive transparent conducting oxides (TCOs) (the second category of *Metal oxides*), represent a promising solution for semiconductor protection in liquid electrolyte. Despite the apparent difficulty of obtaining long-term stability in alkaline electrolytes due to corrosion [38, 106], some researchers [107] have demonstrated good stability of fluorine-doped tin oxide (FTO) on silicon. Mirletz *et al* [108] applied different environmental stressors to commercial TCOs to investigate their degradation. They concluded that the amount of exposure to UV and humidity are the main factors affecting durability. In particular, they observed a yellowing of the TCOs, with a consequent decrease of transparency and increase of resistivity.

The third category of *Metal oxides*, catalytically active metal oxides, has the dual function of protection and catalysis [109, 110], but the protective layer can suffer from electrochemically induced porosity (due to imperfections during the deposition process), locally exposing the semiconductor surface to the aggressive electrolyte [32]. Some rare catalysts such as Ir or IrO_x can also provide this dual functionality [101].

Semiconductor protection can be further refined by a combination of the different categories of protective materials in order to separate the functions of protection, conduction, and catalysis. Adaptation and improvements in the deposition technique (PVD, CVD, ALD, ED, SD, CB) can also further improve the performance and stability of the protective film [111, 112].

Assessment and characterization of corrosion can be experimentally done using techniques such as microscopy, profilometry, XPS, XAS, XES, IPES, UPS, SECM, RBS, AFM and SIMS [100, 113, 114]. These techniques allow the study of the morphological evolution of semiconductors when exposed to PEC operation. Inductively coupled plasma mass spectroscopy (ICP-MS) can be used to measure the dissolved species concentration in the electrolyte.

3.1.2. Intercalation and hydroxylation. Intercalation is the penetration of protons in the semiconductor lattice when free electrons are available at or near the surface [95]. It can induce a perturbation of the charge transport mechanisms in semiconductors. For example, in TiO_2 it increases the activation energy [115]. As a consequence, it induces a decrease of the photocurrent. Calero *et al* [116] studied the impact of proton intercalation on WO_3 performance, observing that intercalation reduces photoactivity. This could be considered a reversible degradation when deintercalation is observed, or an irreversible degradation when it induces irreversible changes in the lattice [117], affecting proton discharge kinetics.

Surface hydroxylation at the SC-liquid EL interface is a reversible chemical destabilization reaction [95, 118]. It is the specific and continuous adsorption and/or desorption of proton and/or hydroxide species:

$$\text{Protonation reaction}: M - \text{OH} \rightarrow MO^- + H^+_{(aq)} \tag{6}$$

$$\text{Deprotonation reaction}: M - \text{OH} + H^+_{(aq)} \rightarrow M - OH^+_2 \tag{7}$$

Surface hydroxylation affects the charge and potential distribution at the semiconductor interface. It can be considered a reversible degradation, but depends on the timescale of the dynamic equilibration which itself depends on pH and the Bronsted acidity of the surface.

Varying strategies can be used to mitigating degradations at the SC-liquid EL interface. The first strategy is the development of new materials and new synthesis techniques to produce stable photoabsorbers. The second strategy consists of developing advanced semiconductor-semiconductor heterojunctions [119] and/or advanced coating techniques like nanocoating, quantum dots, and photodeposition, which allow a considerable increase in stability [120–123]. The integration of co-catalysts [99] or the hybridization of the semiconductor with other materials [124] can also help to improve the stability of the SC-liquid EL interface. The final strategy consists of developing appropriate control techniques for local operating conditions (current density, temperature, acidity) of the device, which highly impact degradation kinetics.

3.2. Semiconductor-metal interface

At the semiconductor-metal interface (see Designs B and C), where a metal ribbon is used for current collection at the semiconductor, the main degradation mechanisms are ribbon wire dry corrosion and ribbon cracking [125–127]. Temperature and humidity are the two main factors which highly affect the semiconductor-metal interface degradation [128]. The consequence is an increased electrical contact resistance between the semiconductor and metal ribbon. Changes in temperature and humidity can also induce metal migration through the interface, with a resulting decrease in shunt resistance of the photoabsorber. Metal migration can also occur at the semiconductor-metal interface between the photoabsorber and the metallic catalyst, significantly affecting catalyst performance.

3.3. Chemical destabilization of the bulk semiconductor

Chemical destabilization is the change in semiconductor crystallinity, grain size, and composition, resulting from the accumulation of photoexcited charge carriers in the lattice. Chemical destabilization is a purely kinetic effect. It can hinder self-passivation of the photoelectrode and consequently result in the dissolution of bulk material. Toma *et al* [114] studied chemical destabilization for bismuth vanadate photoanodes, which are known to be thermodynamically stable against anodic decompositions. They observed a reduction of photoelectrode thickness during testing, with an increasing difference in chemical composition between the bulk and the surface. Thus, the modification of bulk properties induces concentration gradients between the bulk and the surface. Such gradients potentially induce mechanical stresses, further intensifying degradation. The chemical modification of the surface also reduces its catalytic activity for water oxidation. Surface modification is accelerated by higher photocurrents and a higher pH (accelerated in alkaline conditions). Degradation studies focusing on chemical destabilization [114] have shown a rapid increase of the photocurrent during the first 10 s, followed by an anodic shift of the photocurrent onset potential (about 0.1 V after 1 h at pH = 6.8 and 20 min at pH = 12.3), and a decrease of the current density and fill factor.

3.4. Other degradation mechanisms of the semiconductor

The study of the degradation of semiconductors is complex because it strongly depends on the evolution of semiconductor electronic structure. Changes in key physical parameters, such as the mobility of charge carriers or the density-of-states, are directly related to the evolution of electronic band structure.

Depending on cause, different degradation modes are typically classified into [129]: (i) potential induced degradation, which induces an increase of the leakage current, (ii) light induced degradation, which induces an increase of the recombination current, and (iii) ultraviolet induced degradation, which can change the short circuit current and the resistances. Depending on operating conditions, there exist other degradation mechanisms like electromigration, time dependent dielectric breakdown, hot carrier injection, surface inversion, and stress migration in the semiconductor [130]. The models used to describe such degradation phenomena follow an Arrhenius type degradation. Due to the complexity of the degradation phenomena, empirical correlations considering different degradation modes are often used in the photovoltaic cell community [126, 129]. For example, Hacke *et al* [131] proposed the Hereunder equation, based on Peck's model [132], to describe the maximum power degradation:

$$P_{\max}(t) = P_{\max}(0)\left(1 - A\mathrm{e}^{-\frac{E_a}{kT}}RH^B t^2\right) \tag{8}$$

where $P_{\max}(0)$, RH, E_a and k are the initial power, relative humidity, thermal activation energy of the degradation process, and Boltzmann constant, respectively, and B depends on the material and can be obtained experimentally.

Note that the time constants for those degradation mechanisms are much lower than for those of degradation at the direct SC-liquid EL interface, occurring in Designs A and B. Urbain *et al* [37] studied the short term light-induced degradation of a PEC cell for a thin film silicon solar cell interfacing with a liquid electrolyte. They concluded that light-induced degradation is negligible compared to the degradation resulting from photoelectrode corrosion.

3.5. Catalyst

The degradation of the catalyst largely depends on its material, its deposition technique, and its support. Various platinum group metals (PGM) and non-PGM catalysts [77, 133] have been investigated for the water-splitting redox reactions, but only a few of them simultaneously fulfill the requirements of low overpotential, high selectivity, and good stability. McCrory *et al* [134, 135] evaluated the performance and the short-term stability (2 h) of 18 HER catalysts and 26 OER catalysts in acidic and alkaline solutions (1 M H_2SO_4 and 1 M NaOH) at a reference current density of 10 mA cm^{-2}. The high performing catalysts were: Ru, Ir, and Co-based compounds for the oxygen evolution reaction, and Pt, NiMo, and CoMo for the hydrogen evolution reaction. They concluded that there was no particular impact of acidity on anode catalyst degradation. Only noble metal based materials showed promising stability for cathodic catalysts in an acidic environment.

Here we discuss the main degradation mechanisms occurring in the catalyst layer: (i) catalyst support corrosion, (ii) catalyst dissolution, (iii) catalyst agglomeration, and (iv) catalyst poisoning. All catalyst degradation mechanisms induce a loss of exchange current density and an increase of the Tafel slope. Experimentally, these mechanisms can be studied *in situ* using cyclic voltammetry or electrochemical impedance spectroscopy to measure the electrochemically active surface area and resistances, and *ex situ* using scanning electron microscopy for visualization of catalyst particle size and structure.

3.5.1. Catalyst support corrosion. In Design C, a catalyst support is used to ensure good electrical contact between the porous transport layers and catalyst particles. Given the harsh environment (high potential for the anode, high temperature and RH) in which the redox reactions occur, the catalyst support corrodes. This causes a loss of contact between the catalyst and the electrode, a reduction of the catalyst layer thickness, and changes to catalyst surface morphology. In consequence, it induces a decrease of the electrochemically active surface area (generally increasing the activation overpotential) and an increase in the electrical contact resistance.

3.5.2. Catalyst dissolution. Catalyst dissolution is the loss of catalyst particles due to corrosion and/or photocorrosion, and is relevant for all three designs considered. For design C, no photocorrosion occurs. High potentials as well as potential cycling (during short-time transients) are known to have a high impact on the catalyst dissolution rates [136, 137]. Another parameter strongly impacting the dissolution rate is pH. Precious metal

oxides like IrO_2 and RuO_2, which are generally used as the anode catalysts, are stable in acids and unstable in bases. There is good stability when catalyst particles are in contact with metal oxides such as TiO_2 [76] or with other catalysts [138]. Catalyst dissolution is usually higher at the beginning of life, and tends to stabilize after [26]. This is a result of the reorganization of the particles during initial operating hours.

3.5.3. Catalyst agglomeration. Catalyst agglomeration is the increase in size of single catalyst particles due to sintering or due to an increase in the crystal size with time. It is relevant for particle-based catalysts. Catalyst agglomeration induces a reduction in the exchange current density [139], and highly depends on temperature, humidity, and potential [140]. The sintering can occur via Ostwald ripening and/or via coalescence [141]. During Ostwald ripening, small particles dissolve, migrate, and redeposit on bigger particles, inducing a reduction of the electrochemically active surface. In coalescence, small particles sinter together to form bigger particles. For Design A, agglomeration of the catalyst can lead to local opacification of the semiconductor.

3.5.4. Poisoning by foreign ions (catalyst deactivation). The presence of some ions such as Cu^{x+}, Mo^{x+}, Ag^{x+}, Cd^{x+}, Sn^{x+}, and Pb^{x+} (corrosion products or coming from the feed water) can significantly poison the catalyst surface (under potential deposition), leading to an increase in the activation overvoltage, a loss of tolerance, and a decrease in the exchange current density [139, 142]. Fortunately, under potential deposition (UPD) is negligible on IrO_2 and RuO_2 surfaces [46].

This degradation phenomenon is reversible. When immersed in the liquid electrolytes (e.g. H_2SO_4 solution), the impurities can be removed and the catalyst layers can be reactivated [143, 144]. Therefore, poisoning by foreign ions should be lower in Designs A and B given that the catalysts operate in continuous contact with liquid electrolytes. When impurities are removed, the catalyst is again susceptible to dissolution and deactivation. In Design C, the supported catalyst layer would have to be removed and treated in a liquid electrolyte before reintegration into the device. Sonification in CCl_4 is also a good technique to clean fouled electrodes [145]. However, the contamination of the anode catalyst layer by species like titanium, possibly coming from the semiconductor, bipolar plates, and porous transport layer, would induce a decrease in anodic exchange current density over time.

To mitigate the catalyst degradation, some researchers focus on the optimization of particles size and dispersion [146], while others focus on the development of stable mixed catalysts [147]. The integration of additives in the catalyst layer can also help to reduce the catalyst dissolution and agglomeration [148–151]. With regard to catalyst support, stabilization techniques include the development of novel carbon support structures [152, 153], and the development of hybrid (carbon/non carbon) supports [154], which are resistant to high potentials. According to Rozain *et al* [155], the use of micron-sized titanium particles as support for catalysts, such as IrO_2 particles, is a promising technique to increase stability against corrosion.

Furthermore, the device design should avoid local current concentrations because high current densities promote the loss of catalyst material in the concentration zone, which is detrimental to the durability of the entire device [156]. During operation, catalyst degradation can be mitigated using an appropriate control strategy limiting the potential cycling of the cell, stemming from short-term transients of incoming irradiation. Note that potential cycling highly accelerates catalyst dissolution [136, 137].

3.6. Electrolyte

During PEC operation, physical and chemical changes occur in the electrolyte, whether liquid or solid, which greatly affect the ionic conductivity and/or product separation. Assuming that (in the design choices relevant for a practical application) we deal with a flowing system (in contrast to a batch-type system), the liquid electrolyte is continuously flowing, providing reactants and removing products at the same time, and is potentially cleaned and recirculated. Primary degradations are related to pollution, salts deposits, and saturation [69, 74, 157]. Pollution is chiefly due the dissolution of impurities in the electrolyte. Those impurities can come from the feed water and from the corrosion of different PEC components. They can also be produced in the electrolyte itself through side reactions. For instance, in alkaline electrolytes, polluting ions can be oxidized when the current density reaches the limiting current of the hydroxyl ions [158]. The impurities—metal ions—can also induce salt deposits, which are governed by their own solubility product constants [69]. Evolution of gaseous products due to the accumulation and supersaturation of the produced gas in the electrolyte increases the ionic transport resistance. Gas bubbles can be trapped in the electrolyte, causing obstruction to catalyst access. All these effects increase ionic transport losses in the electrolyte and reduce the purity of produced hydrogen.

Degradation at the SC-liquid EL interface was discussed in section 3.1, with an indication of the impurities which might affect the electrolyte. Impurity composition can be analyzed via ICP-MS.

Alkaline diaphragms are known to have acceptable chemical and mechanical stability but exhibit poisoning or pollution from foreign ions [69, 159]. Proton exchange membranes (e.g. Nafion®) suffer from chemical, mechanical, and thermal degradations. Here we discuss them in more detail. The degradation of solid electrolyte can be studied *in situ* using voltammetry or impedance spectroscopy to measure gas permeation across the membrane and *ex situ* using electron microscopy.

3.6.1. Chemical degradation. The chemical degradation mechanism occurring in the Nafion® membrane during electrolysis was accurately described and modeled by Chandesris *et al* [160]. During operation, there is a continuous oxygen crossover from the anode to the cathode compartment. This permeating flux increases with temperature and decreases with current density. On the cathode side, the reduction of the permeated oxygen competes with the hydrogen evolution reaction. As a consequence, hydrogen peroxide (H_2O_2) forms.

In the presence of metal ion impurities, like Fe^{x+}, hydrogen peroxide (H_2O_2) is decomposed into hydroxyl (HO) and hydroperoxyl (HOO) radicals [161] via Fenton's reaction [162]. There is a subsequent degradation of the perfluorosulfonic acid backbone of the membrane with a resulting fluoride and sulfur release, and a membrane thinning (mostly at the cathode side). Thus, the dissolved species coming from the corrosion of the semiconductor and/or bipolar plates can directly catalyze the chemical attack of the membrane. This degradation mechanism leads to an exponential increase of gas crossover, and can also lead to membrane failure. It therefore significantly affects the reliability of the device.

Chemical degradation largely depends on operating temperature. According to Chandesris *et al* [160], the fluoride release rate (FRR) increases from 0.25 to 1.7 $\mu g/h/cm^2$ at 1 A cm^{-2} when the temperature changes from 60 °C to 80 °C. The fluoride anions produced are very aggressive and contribute to an increased corrosion rate of other components.

The chemical degradation can be studied experimentally *in situ* by measuring FRR and the sulfur emission rate (SER) in the effluent water, and *ex situ* by measuring the thickness of the membrane at the beginning and end of life. The polymer membrane also suffers from photolysis [163], which is the chemical process whereby a chemical compound is broken by incident photons, resulting in lower molecular weight molecules. This change has negative consequences on the ionic conductivity and refractive index of the membrane. According to Fox *et al* [164], the dose of exposure to radiation plays an important role in Nafion® membrane degradation. Gamma rays are particularly responsible for chemical degradation, with a consequent fluoride release.

3.6.2. Poisoning (deactivation due to crosslinking by metal ions). Metallic ions (Fe^{x+}, Ni^{x+}, Cr^{x+}, Cu^{x+}, Pb^{x+}) are the most significant membrane poisoners. They are generated during corrosion and additionally come from feed water. Poisoning degradation mechanisms follow three sequential steps [139, 165, 166]:

- Dissolution: the metallic ions are dissolved into the membrane via diffusion and permeation;
- Contamination: the metallic ions occupy the ion exchange sites of the polymer membrane and in the catalyst layer ionomer;
- Poisoning: since the metal cations migrate slower than protons, the contaminants lead to higher ohmic losses.

Membrane poisoning by metallic ions can be reversed by bathing in sulfuric acid solution.

A second group of relevant membrane poisoners are dissolved catalyst particles. These particles can easily precipitate into the membrane, inducing metallization. The associated mechanism, described by Grigoriev *et al* [167], is characterized by the following:

- Dissolution: the catalyst particles are dissolved during operation (see section 3.3);
- Diffusion: the dissolved catalyst particles diffuse into the membrane as cationic species;
- Migration: the cationic species migrate towards the cathode because of the electric field;
- Precipitation: at a certain distance from the anode, the cationic species react with dissolved hydrogen which cross-permeates from the anode, chemically reduced into insoluble particles. As a consequence, a metal layer forms in the membrane parallel to the surface.

This degradation mode induces a change in the catalyst-electrolyte interface and, consequently, an increase of the capacitance of the double layer [168]. The capacitive behavior of the interface depends on interface roughness, crystallinity, and anion adsorption.

3.6.3. Mechanical degradation. In PEC devices, there is mechanical degradation of the membrane resulting from hydrothermal stresses. The membrane is generally a thermoplastic material undermined by temperature, humidity, and pressure cycling. Water is necessary for ion conduction, but its absorption by the membrane induces swelling. A polymer membrane expansion of 11% has been measured by Grigoriev *et al* [167]. During operation, the membrane also changes in crystallinity [169], which impacts ionic conductivity.

If exposed to solar radiation, membranes suffer from phototendering, inducing losses in strength and flexibility [163]. According to Iwai *et al* [170], high doses and large rates of gamma rays promote weakening and embrittlement of Nafion® material. Conti *et al* [171] conducted a time-resolved paramagnetic resonance investigation of Nafion® and concluded that UV rays generate excited triplet states, accelerating degradation.

Excluding the development of innovative solid electrolytes, such as radiation-grafted membranes, SPEEK (sulfonated polyetheretherketone), and SPSF (sulfonated polysulfone), etc [172], the degradation of membranes can be mitigated by using additives to improve mechanical strength [173] and chemical stability [174]. Consistent heat management of the device should be ensured in order to avoid the formation of hot spots, which severely accelerate solid electrolyte degradation [47, 175].

3.7. Other components

Compared to the other designs presented in figure 1, in Design C there are two additional components: (i) conductive flow field plates, and (ii) porous transport layers. Conductive flow field plates, usually called bipolar plates, are multifunctional components simultaneously ensuring charge carrier transport from the semiconductor to the catalyst, the supply of reactant (water), removal of produced gases from the cell, and the mechanical stability and integrity of the device. The plates should consequently exhibit good electrical conductivity, good mass transport in the integrated channels, low cost, good mechanical strength, and good durability. Stainless steel is a less expensive alternative, but it corrodes very quickly in a highly acidic environment. For that reason, if used, steel is usually coated with titanium or platinum [176]. This coating, while successful in reducing corrosion, increases the electrical

resistance [177]. Titanium is a more costly alternative for flow field plates. It has good corrosion resistance, but evolves a passive oxide layer during the first few operating hours, greatly increasing the electrical contact resistance [178, 179]. Another degradation mechanism reported in literature is the hydrogen embrittlement of the cathode plate through the diffusion of hydrogen in the metal, with a subsequently increased probability of fracture [180]. Nitridation is an excellent method to prevent H_2 embrittlement of Ti plates.

The porous transport layer (PTL) is usually made of carbon (paper or cloth) or metal material (felt, powder, or mesh). Porous transport layers mainly suffer from chemical degradation due to corrosion, and by erosion due to water flow [181]. Corrosion is more severe at the anode compartment due to the combination of high potential and high oxygen concentration. For this reason, metallic materials are usually preferred as the anode PTL. Mo *et al* [182] tested a stainless steel mesh as the anode PTL, but they observed a high corrosion rate, with a high transport of irons from anode to cathode, polluting the membrane and catalyst layers. Titanium meshes, felts, and foams are the most durable approaches, thanks to their resistance to corrosion [183]. However, titanium based porous layers also suffer from a passive oxidation layer, which reduces performance. The use of platinum or gold-based coatings prevents dramatic increases in electrical resistance, but engenders additional costs.

PTLs also suffer from mechanical degradation: interface delamination and fiber cracks. Interface delamination is caused by freeze and thaw cycles. The processes of ice formation and melting in the pores induce cycles of expansion and compression in the fibers, leading to delamination [184]. Fiber cracks, which highly degrade electrical conductivity, are caused by a local overcompression of the fibers [185]. In fact, good clamping pressure is necessary to achieve solid electrical contact between the bipolar plates and the PTL, but this pressure is heterogeneous over the active area due to the channel-rib structure of the bipolar plates.

The PTL can also suffer from pollution and gas starvation, caused by the accumulation of solid particles or gas bubbles in PTL pores. Solid impurities, which come from corrosion products or from feed water can block the reactant supply and the removal of products, resulting in an increase in the mass transport resistance of the device. Indeed, pore size and structure greatly affect fluid transport [186]. Gas starvation in the pores leads to obstruction of the reactant and product diffusion pathways, decreasing the overall performance of the device [187].

3.8. Overview of degradation mechanisms

An overview of the different degradation mechanisms presented above, as well as the interplay between the different components is presented in this section. In figure 2(a), degradation mechanisms are organized according to the components and interfaces affected. Intrinsic degradations of components are indicated with red circles, while degradations arising from the degradation of other components are circled in green.

Design B is used for illustration, so catalyst photocorrosion as well as corrosion of bipolar plates and porous transport layers are missing from the figure. Note that in contrast to Design A, Design B doesn't endure catalyst and electrolyte photo-driven degradation processes (photocorrosion, photolysis, phototendering, etc). In figure 2(b), the interplay between the degradation effects of different components is presented. At the center of the semiconductor-electrocatalyst-electrolyte triangle is solar radiation.

Direct interaction between the photons and various components is responsible for several degradation mechanisms specific to photo-driven applications. There are different ways to classify and quantify those degradations and their impact on device lifetime.

3.8.1. Degradation classification. There are two different classes of degradation, depending on their consequences to device performance:

i. Progressive performance loss (durability).
   This first category of degradation can be observed *in situ* during experimentation and can be classified into two subgroups:
   - *Reversible degradation:* when the lost performance can be recovered using alternative methods. For instance, dynamic effects in the semiconductors (capacitive charging, intercalation etc.) can be recovered during dark periods, and electrolyte and catalyst pollution by ions (deposits, passivation) can be recovered by sweeping the device with an appropriate cleaning fluid in order to remove impurities
   - *Irreversible degradations:* when lost performance cannot be recovered. Examples are semiconductor passivation, catalyst dissolution, and structural changes.

ii. Sudden loss of functionality due to failure (reliability).
   The second category of degradation refers to an instantaneous drop in performance. The principal mechanism causing sudden device failure is local perforation of the solid electrolyte/separator and successive catalytic recombination of hydrogen and oxygen. Photoelectrode dissolution, cracks, and pinholes can also lead to a sudden loss of functionality above a certain threshold, without any previous sign of performance decrease. It is worth mentioning that the initiation of this kind of degradation can lead to punctual performance increase until the failure results. For example, the chemical degradation of the membrane induces its thinning, and in consequence a decrease of the ionic transport resistance up until failure. This kind of degradation is a considerable challenge to device reliability.
   Besides degradation of individual components, an interplay exists between the different degradation products. For example, metal ions coming from the dissolution of the photoelectrode can catalyze chemical degradation of the polymer membrane.

Finally, addressing the durability and reliability issues in PEC devices requires tackling degradation at two timescales:

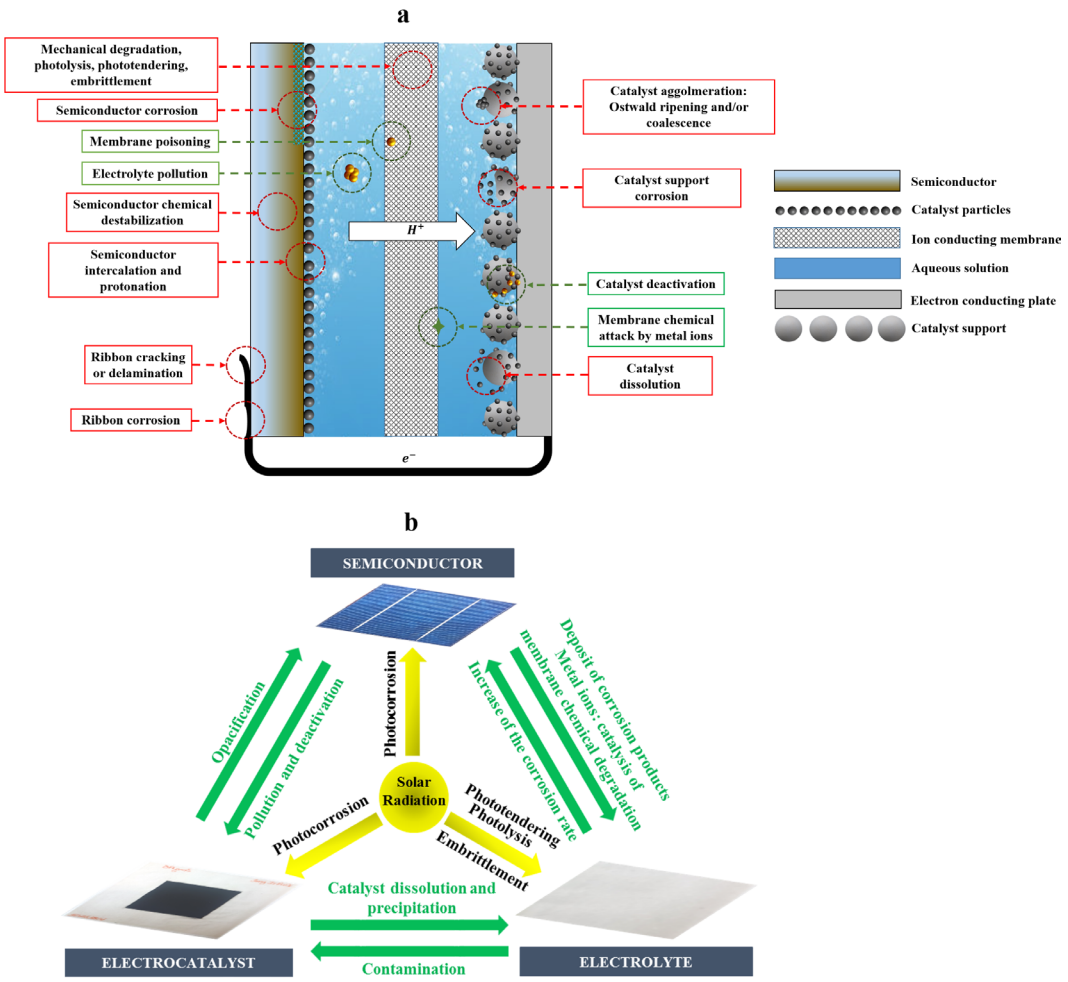

Figure 2. Overview of various degradation mechanisms. (a) Degradation mechanisms occurring in the different components and at the interfaces using Design B for illustration. (b) Interplay between the degradation effects of different components.

- *Short-term* issues are mainly concerned with the stability of photoelectrodes, and are fundamentally important and urgent due to a timescale of only a few hours (for unstable photoelectrodes with solid-liquid junctions).
- *Long-term issues* are mainly concerned with the stability of catalysts, membranes, and the integrated device. Guidance for these issues can be gleaned from fuel cell and electrolyzer research communities and industries developing highly stable catalysts and electrolytes.

3.8.2. Degradation quantification. Degradation must be quantified in order to: define end of life criteria, evaluate device durability, and compare long-term device performance. Many authors have used the photocurrent stability to quantify device stability and define device lifetime. This approach is reasonable only for Designs B and C. For all designs, a measurement of the hydrogen production rate, the oxygen production rate, and the detection of products from side reactions, provides a more conclusive indication of degradation and affords possibilities for diagnosis of degradation mechanisms. End of life can be defined as the time at which the ratio between the instantaneous STH efficiency and its initial value reaches a certain threshold (for example 80%).

4. Durability prediction in integrated devices

4.1. Modeling approaches

There are two major approaches to degradation modeling in photoelectrochemical devices, macroscopic approaches or physics-based approaches. Macroscopic approaches (top-down approaches) with empirical correlations can be used to relate operating conditions to the performance loss. This approach requires extensive (and therefore time intensive) experimental investigations of various materials and components in integrated PEC device setup. Physics-based degradation models (bottom-up approaches) can be developed, on the other hand, incorporating smaller-scale phenomena. These small-scale models are coupled to a macroscopic scale device model to provide a deeper physics-based understanding of degradation. Such approaches are regularly used in the fuel cell and electrolyzer community

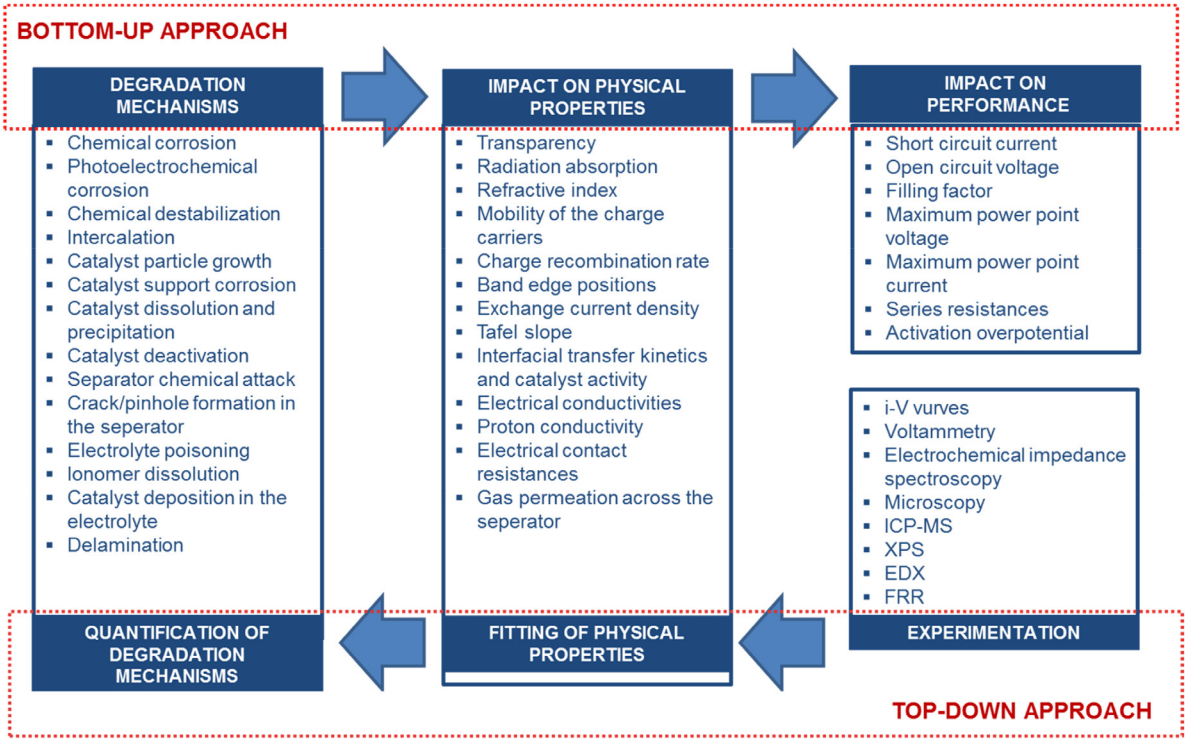

Figure 3. Different approaches to degradation investigation in PEC cells.

[188]. This approach requires a detailed understanding of the fundamentals of material science and solid state physics. Both approaches are illustrated in figure 3.

In the *bottom-up* approach, the main challenge is the investigation of the impacts of different degradation mechanisms on the physical properties of the different components. These can be modeled at varying scales: atomistic, molecular, coarse grain, and continuum level [189], or experimentally measured via accelerated stress tests on individual components.

In the *top-down* approach, the main challenge is related to the implementation and testing of various materials and components in integrated PEC devices utilizing different design options, under a large range of realistic operating conditions. Additionally, the assessment and quantification of degradation in such measurements is challenging. The best indicator of device degradation utilizing this approach is the temporal evolution of STH efficiency. Degradation of the STH efficiency, however, results from the convoluted interplay between the degradation of various components (semiconductor, electrolyte, catalysts) and their interfaces. Additional detailed diagnostics of the components can be done *in situ* or *ex situ*.

4.2. An illustrative case study using a bottom-up approach

We utilize a *bottom-up* approach (without directly modeling of the degradation mechanisms) to develop a simplified PEC device model accounting for degradation, in order to quantify PEC device performance loss and gain insight into the design-dependence of degradation behavior.

Performance loss in the semiconductor can be observed and quantified through the short circuit current, I_{sc}, linked to a decrease in the fill factor, FF [190]. Other observable parameters are the increase in series resistance, r_s, and the decrease in shunt resistance, r_{sh}. Variation in r_s is related to a change in the electrical conductivity of the material, and an increase in the recombination rate. Variation in r_{sh} is related to changes in crystallinity, changes in contact resistance at the metal-semiconductor interface, and metal migration through the interface. A decrease in the photogenerated current, i_{ph}, due to a change in the absorption behavior of the semiconductor, and an increase of the reverse diode saturation current, i_d, is also observed. As a consequence, the open circuit voltage, V_{oc}, decreases, resulting from a loss in the ability of the junction to separate the electrons and holes.

Performance loss in the integrated electrolyzers is often observed through an increase in the potential losses in the system. Reversible degradation effects account for up to 61% of the total voltage increase, and are more pronounced at high current densities [139]. Irreversible degradation effects are often related to an increase of (i) ohmic resistances (corrosion and passivation of the plates, increase of the membrane ionic resistance), (ii) transfer resistance in the catalyst layers resulting in a decrease of the exchange current density, i_0, and (iii) the Tafel slope, b, due to catalyst dissolution, or/and deactivation and pollution. Usually, greater degradation and resulting potential losses over time are observed in the anodic catalyst. However, degradation of the cathodic catalyst can also play a significant role [137]. Generally, the Tafel slope does not significantly increase during operation [191], but large changes in catalyst particle size and structure can affect it considerably. Furthermore, the chemical degradation of the membrane induces an increase of the hydrogen permeation, with a resulting reduction in efficiency. One fundamental difference between commercial electrolyzers and electrolyzers

operating in wired PEC cells is the operating current density. While the former operate at current densities around 1 A cm^{-2}, the latter operate at around 10 mA cm^{-2}. Cost advantages are usually observed for larger current densities (reduced use of components). In order to reach high current densities in PEC cells, radiation and/or current concentration can be applied [1, 192]. Generally, measured performance loss is larger at high current densities [193]. In contrast to commercial electrolyzers, degradation of the electrochemical surface area of the catalyst in PEC devices (related to the exchange current density) has more impact on performance than the reduction of the electronic activity of the catalyst (related to the Tafel slope, which indicates how much the overpotential needs to be increased in order to increase the reaction rate). Another fundamental difference between the commercial electrolyzer and the PEC device is the instability caused by the solar profile, which can induce extreme dynamics in PEC cells. Those dynamics are known to accelerate degradation of the electrolyzer [138].

The simplified equations describing the buried photoabsorber and the integrated electrolyzer are [47, 194]:

$$\begin{cases} i = i_{\mathrm{ph}} - i_{\mathrm{d}}\left[\exp\left(\dfrac{e(U+ir_{\mathrm{s}})}{nkT}\right)-1\right] - \dfrac{U+ir_{\mathrm{s}}}{r_{\mathrm{sh}}} \\ \quad \text{(Photoabsorber)} \\ U = U_{\mathrm{ocv}} + b_a \ln\left(\dfrac{Fi}{i_{0,a}}\right) + b_c \ln\left(\dfrac{Fi}{i_{0,c}}\right) + r_{\mathrm{E}} F\, i \\ \quad \text{(Electrolyzer)} \end{cases} \tag{9}$$

where n is the ideality constant of the diode, i the operating current density, U the operating voltage, and U_{ocv} the equilibrium potential of the two water electrolysis half-reactions. The current dilution factor, F, is used to take into account the ratio between the photoabsorber and the electrolyzer areas [1]. i_{ph} and i_{d} are calculated using the following relations [1]:

$$i_{\mathrm{ph}} = C i_{\mathrm{sc},0} \frac{\phi}{\phi_0} \tag{10}$$

$$i_{\mathrm{d}} = i_{\mathrm{sc},0}\left(\exp\left(\frac{eV_{\mathrm{oc}}}{kT}\right)-1\right) \text{ with } V_{\mathrm{oc}} = V_{\mathrm{oc},0} + \frac{kT}{e}\ln\left(C\frac{\phi}{\phi_0}\right) \tag{11}$$

where $i_{\mathrm{sc},0}$ and C are, respectively, the short circuit current in the reference conditions (1000 W m^{-2} with no concentration) and the radiation concentration (defined as the area between the radiation collector and the photoabsorber). V_{oc} and $V_{\mathrm{oc},0}$ are, respectively, the open circuit voltage in the operating and in the reference conditions. ϕ and ϕ_0, respectively, represent the mean operating radiation flux (assumed 300 W m^{-2}) and the reference radiation flux (1000 W m^{-2}).

We collected degradation rates found in literature for separated photovoltaics cells and electrolyzers due to a lack of measured PEC degradation data. We believe they provide an interesting starting point into the investigation of integrated PEC device degradation. Generally, the degradation of i_{ph}, r_{s}, r_{E} and r_{sh} are linear, while the degradation of i_{d} is exponential with time [195, 196]. The variation of i_0 is usually higher at the beginning of life due to catalyst particle reorganization during the first operating hours. In this study, we assumed linearized evolution of all degradation parameters, according to:

$$p = p_0(1 + Kt) \tag{12}$$

where p and p_0 are, respectively, the value of the physical quantity at the time t (in hours) and at the beginning of life. The values of the annual degradation rates, K, are collected from experimental and modeling results in literature [47, 138, 139, 143, 195–201]. The chosen reference parameters are presented in table 2.

Table 2. Different parameters used in the model. The initial values represent the values of the physical parameters at the beginning of life. Three different types of semiconductor can be used, depending on the design (SC 1, SC 2, and SC 3). Minimum, mean, and maximal values are used in order to study the impact of the degradation rates of single components on device performance.

Parameter $\boldsymbol{p}$ (units)	Initial value $\boldsymbol{p}_0$	Degradation rate $\boldsymbol{K}$ ($\times 10^{-5}$ h^{-1})		
		Minimum	Mean	Maximum
$i_{\mathrm{sc},0}$(A m^{-2})	SC 1: 191 SC 2: 191 SC 3: 196	−0.2	−0.35	−0.5
V_{oc} (V)	SC 1: 1.79 SC 2: 2.01 SC 3: 2.32	−0.1	−0.2	−0.3
r_{s} (Ω m^2)	SC1 and SC3: $3 \cdot 10^{-3}$ SC 2: $3 \cdot 10^{-5}$	+0.5	+1.75	+3
r_{sh} (Ω m^2)	2	−1	−2	−3
$i_{0,a}$ (A m^{-2})	$2 \cdot 10^{-2}$	−0.25	−1.35	−2.5
$i_{0,c}$ (A m^{-2})	10	−0.25	−1.35	−2.5
b_a (mV dec^{-1})	47	No degradation	+0.5	+0.5
b_c (mV dec^{-1})	30	No degradation	+0.5	+0.5
r_{E} (Ω m^2)	$2 \cdot 10^{-5}$	+4.4	+25	+40

Table 3. Degradation rates of the physical parameters used for the different designs.

Parameter $\boldsymbol{p}$ (units)	Degradation rate $\boldsymbol{K}$ ($\times 10^{-5}$ h^{-1})		
	Design A	Design B	Design C
i_{ph}(A m^{-2})	Max	Mean	Min
V_{oc} (V)	Max	Mean	Min
r_{s} (Ω m^2)	Min	Max	Max
r_{sh} (Ω m^2)	Min	Max	Max
$i_{0,a}$ (A m^{-2})	Max	Mean	Min
$i_{0,c}$ (A m^{-2})	Max	Mean	Min
b_a (mV dec^{-1})	Mean	Mean	Min
b_c (mV dec^{-1})	Mean	Mean	Min
r_{E} (Ω m^2)	Min	Min	Max

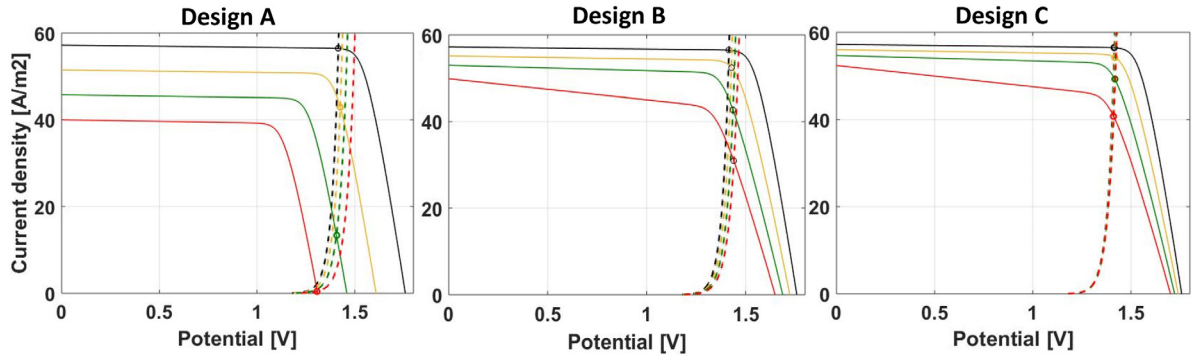

Figure 4. Evolution of the *i*–*V*-curves during the first 30000 h of device operation for the three different designs, all for SC1. The black, yellow, green, and red lines correspond to 0, 10000, 20000, and 30000 operating hours. Circles indicate operating points at the different times.

The change of the ideality factor n is not considered in this study, but it can have non negligible effect on the performance degradation [195].

4.2.1. Impact of the PEC design on performance loss In this section, the impact of PEC designs on performance losses is investigated using the physical parameters presented in table 2. Degradation rates of the physical parameters highly depend on design. In Design A it is supposed that photocorrosion and chemical destabilization at the SC-liquid EL and EC-liquid EL interface induce large degradation rates of i_{ph}, V_{oc}, $i_{0,a}$ and $i_{0,c}$. In Design B, the main accelerated degradation parameters are considered for i_{ph} and V_{oc} due to the photocorrosion and chemical destabilization of the semiconductor, and for r_s and r_{sh} due to the metal wire corrosion and the degradation of the contact between the semiconductor and the wire. In Design C, the main accelerated degradation parameters are the electrolyzer electrical resistance degradation due to increases in the ionic resistance of the solid electrolyte, and the increase of electrical contact resistances between the different components. A summary of the different parameters considered for the different designs is presented in table 3.

Photoabsorbers were chosen based on the ideal performance of a tandem photoabsorber calculated by the Shockley–Queisser limit [202]. Three semiconductor tandems with very similar $i_{sc,0}$ but increasing V_{oc} were chosen utilizing two different band gap semiconductors for each: 1.82/0.6 eV band gaps (SC 1), 1.8/1.2 eV band gap (SC 2), 1.6/1.08 eV band gaps (SC 3). The electrocatalysts chosen are IrO_2, and Pt particles in acidic environments for the anode and cathode catalyst layers, with a loading of 1.5 and 0.5 mg cm^{-2}, respectively. Solid and liquid electrolytes chosen are Nafion® and sulfuric acid, with a mean ionic path length resulting in a resistance of $2 \cdot 10^{-5}$ Ω m^2. Mass transport limits and concentration variations in the electrolytes are neglected.

Evolutions of the current density versus voltage curves (*i*–*V*-curves) during the first 30000 operating hours of the device utilizing SC1, obtained using a typical yearly-mean operating radiation flux (300 W m^{-2} for 24 h a day, 300 K), are presented in figure 4.

Globally, the operating point is very close to the maximal power point of the photoabsorber at the beginning of life. Component choice was deliberately made to ensure this initial operation in order to optimize device design in terms of efficiency and cost. For all designs, the performance degradation rate is lower at the beginning of life but progressively increases. For example in Design B, the degradation of the operating current density is 0.39 mA m^{-2} h^{-1} during the first 10000 h, 0.98 mA m^{-2} h^{-1} during the following 10000 h, and 1.19 mA m^{-2} h^{-1} during the last 10000 h. All device designs continue to show reasonable efficiencies after 30000 operating hours, with the exception of Design A, where efficiency is close to zero at the end of life. Given that the electrocatalysts work near the activation zone (due to the low current densities of the photoabsorber), performance loss is mainly affected by semiconductor degradation. However in Design A, the increase in the activation overpotential, due to electrocatalyst corrosion and photocorrosion, has a high impact on performance loss. In Design B, the activation potential increase is lower, but degradation of the semiconductor induces a very large drop in the operating point. In Design C, degradation of the electrolyzer is mainly due to an increase of the ohmic losses, even though its impact is moderate at these low operating currents. The performance loss is almost entirely due to photoabsorber degradation.

In order to compare the durability of the three designs over their entire lifetime, the cumulated amount of produced hydrogen was computed, considering a yearly mean radiation flux of 300 W m^{-2}. The obtained values for the Designs A, B, and C were 31.6, 52.1, and 57.1 kg m^{-2}, respectively. Thus, Design C is more durable, even though alternative parameters such as materials, geometry, and operating conditions must be considered for a more accurate study.

In order to evaluate the effects of different degradation parameters on performance drop in PEC devices, a sensibility study was also performed. The degradation combinations primarily affecting performance were a change in the absorption behavior of the semiconductor and an increase of the electrolyzer resistance to charge transport. While the former cannot be managed easily, the latter can be limited by using coated bipolar plates and porous transport layers, and by regularly sweeping the electrolyzer with an appropriate cleaning solution to remove impurities. Typically, the

degradation rate K of the electrolyzer's electrical conductivity drops from $40 \cdot 10^{-5}$ to $4.4 \cdot 10^{-5}$ h^{-1} when the titanium components of the cell (bipolar plates, porous transport layers) are coated [139].

The studies presented in figure 4 are obtained for 1 sun (no radiation concentration) and low operating current densities for the electrolyzer. However, radiation concentration is often useful to minimize the cost of the photoabsorber while current dilution is useful for optimizing the operating point of the electrolyzer [1]. The impact of these parameters on durability is detailed in the following section.

4.2.2. Impact of PEC operation on performance loss. Four different operating cases of Design C are investigated in order to evaluate the impact of device geometry on performance loss and lifetime:

> *Case 1*: A design with no radiation concentration and no current dilution (the same as presented above, in section 4.2.1). The areas of the photoabsorber and electrolyzer are the same ($C = F = 1$), and the semiconductor SC 1 is used for the photoabsorber)
> *Case 2*: A design with radiation concentration ($C = 100$) and no current dilution ($F = 1$). Due to the radiation concentration, the photoabsorber and electrolyzer have a smaller area. Compared to case 1, a high open circuit voltage photoabsorber is used (SC 2, presented in table 3) in order to make the electrolyzer function in the 'plateau' region at the beginning of life. High current densities induce high ohmic losses in the electrolyzer, shifting the operating point into the resistance zone of the photoabsorber i–V curve.
> *Case 3*: A design with no radiation concentration ($C = 1$) and a current concentration in the electrolyzer ($F = 0.1$). The advantage of concentrating the current is to have an electrolyzer with a small surface, which operates at a high current density. Compared to case 1, a medium open circuit voltage photoabsorber is used (SC 2 as presented in table 3) in order to make the device operate in the 'plateau' region at the beginning of life.
> *Case 4*: A design with radiation concentration ($C = 100$) and current dilution ($F = 10$). The electrolzyer area is larger than the photoabsorber area. This current dilution allows electrolzyer operation at moderate current densities, avoiding high degradation rates and potential mass transport limitations. As in case 3, a medium open circuit voltage photoabsorber is used (SC 2).

In Case 1, the photoabsorber works close to the conditions of the studies from which we extracted the degradation rate range (1000 W m^{-2}, 300 K). The electrolyzer, however, works at much lower current densities (around 180 A m^{-2}) compared to the conditions of the studies from which we extracted the degradation rate ranges (around 10 000–20 000 A m^{-2}). Moderate degradation rates were utilized since the degradation of the electrolyzer greatly increases in tandem with operating current density.

In Case 2, high degradation rates were used for the photoabsorber as well as for the electrolyzer. The photoabsorber operates at very high irradiations (i.e. 300 000 W m^{-2}) and the electrolyzer at high current densities (around 18 000 A m^{-2}). Those operating conditions, caused by the radiation concentration, increase the degradation rates.

In Case 3, high degradation rates are utilized only for the shunt and series resistances of the photoabsorber. Other degradation rates are moderate. The photoabsorber (SC 2) works at the yearly-averaged irradiation (300 W m^{-2}), while the electrolyzer works at a mean current density (around 1800 A m^{-2}), due to the current concentration between the photoabsorber and the electrolyzer.

In Case 4, high degradation rates are used for the photoabsorber while mean degradation rates are used for the electrolyzer. This design represents the best solution from a techno-economic point of view because it concentrates the radiation on a small area of the photoabsorber (which is costly), and dilutes the current density at reasonable values in a larger area electrolyzer [1]. A summary of the different parameters considered in the four cases is presented in table 4.

The evolutions of the current density versus voltage curves (i–V-curves) during the first 30 000 operating hours of the device, obtained using the yearly mean operating radiation flux (300 W m^{-2}), are presented in figure 5.

In Case 1, the electrolyzer operates in the activation zone and degradation in performance results from ohmic losses. Given that those degradation rates are very low at the given current density (around 55 A m^{-2}), the performance degradation of the device is mainly due to photoabsorber degradation. This configuration allows the achievement of high durability. However, the electrolyzer underperforms, and its hydrogen production rate is very small compared to capacity. Note that for a PEC device working at low current densities (low radiation concentration), an increase of the activation overpotential, which is related to degradations of the exchange current density and Tafel slope (i.e. the catalyst degradation), has more impact on performance degradation than an increase in ohmic losses (i.e. degradation of the electrolyte, passivation layers, etc).

Table 4. Degradation rates of the physical parameters used for the four case studies.

	Degradation rate $\boldsymbol{K}$ ($\times 10^{-5}$ h^{-1})			
	Case 1	Case 2	Case 3	Case 4
Parameter $\boldsymbol{p}$ (units)	$C = 1$, $F = 1$	$C = 100$, $F = 1$	$C = 1$, $F = 0.1$	$C = 100$, $F = 10$
i_{ph} (A m^{-2})	Min	Mean	Min	Mean
V_{oc} (V)	Min	Mean	Min	Mean
r_s (Ω m^2)	Max	Max	Max	Max
r_{sh} (Ω m^2)	Max	Max	Max	Max
$i_{0,a}$ (A m^{-2})	Min	Max	Mean	Mean
$i_{0,c}$ (A m^{-2})	Min	Max	Mean	Mean
b_a (mV dec^{-1})	Min	Max	Mean	Mean
b_c (mV dec^{-1})	Min	Max	Mean	Mean
r_E (Ω m^2)	Max	Max	Mean	Mean

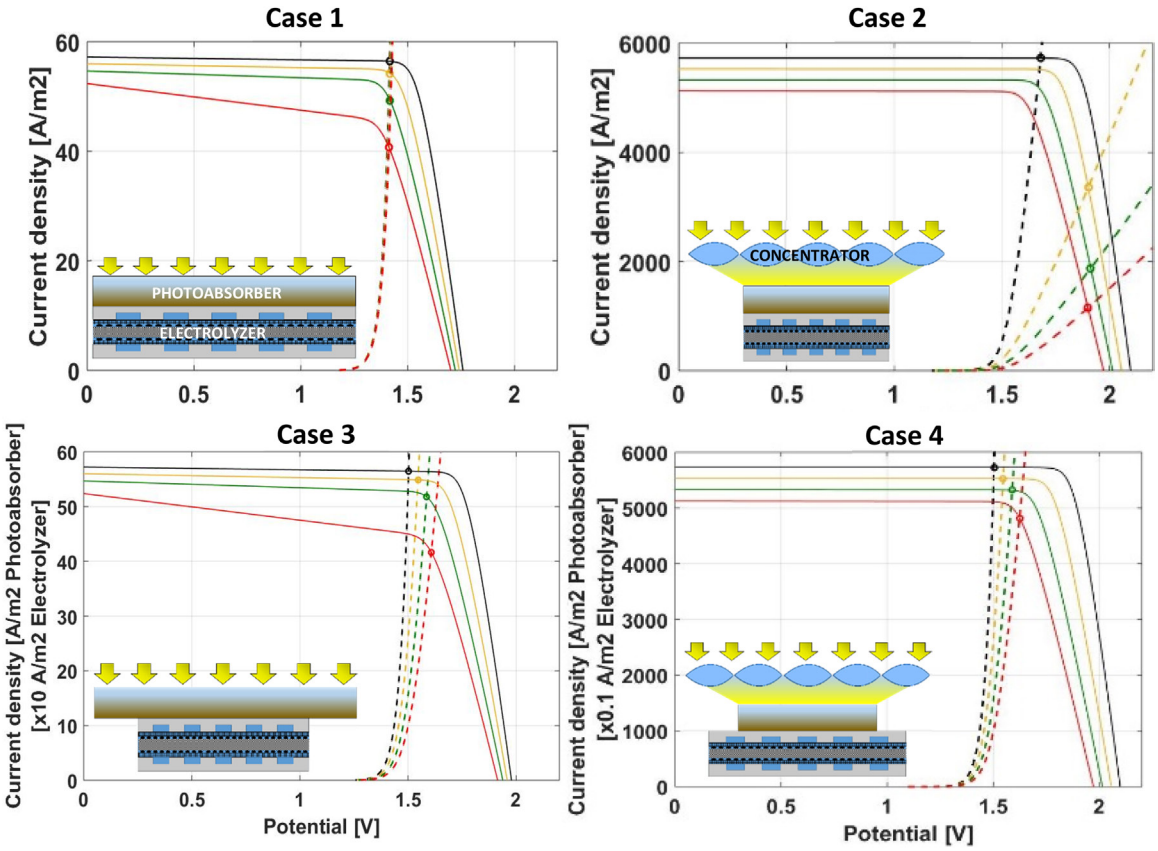

Figure 5. Evolution of the *i–V* curves during the first 30 000 operating hours of the device for four different cases (table 4). Case 1. Design with no radiation concentration and no current dilution ($C = F = 1$). The area of the photoabsorber and electrolyzer are the same. Case 2. Design with radiation concentration ($C = 100$) and no current dilution ($F = 1$). Case 3. Design with no radiation concentration ($C = 1$) and current concentration ($F = 0.1$). Case 4. Design with radiation concentration ($C = 100$) and current dilution ($F = 10$). The black, yellow, green, and red lines correspond to 0, 10 000, 20 000, and 30 000 operating hours. The circles indicate the operating points at different times.

In Case 2, both the photoabsorber and electrolyzer operate at high current densities, accelerating their degradation. The electrolyzer, working in the ohmic zone, is very sensitive to increases in electrical resistances. The largest reduction in current density (0.237 A m^{-2} h^{-1}) is observed during the initial operating hours, followed by a progressive decrease. Thus, for a PEC device operating at high current densities, all degradation mechanisms which increase the electrical or ionic transport resistances (electrolyte poisoning, corrosion of the metal plates, passivation) should be limited as much as possible.

In Case 3, the operating current, which determines the amount of produced hydrogen, decreases slightly during the first 20 000 h, followed by a dramatic drop at a certain threshold, when the device starts to work in the resistance zone of the photoabsorber.

In Case 4, the behavior is very similar to Case 3, even though the irradiation is very different. Thus, current dilution is helpful in moderating performance degradation due to radiation concentration.

The cumulated amount of produced hydrogen, considering a yearly mean radiation flux of 300 W m^{-2}, is 57.1, 32.4, 58, and 60.1 kg m^{-2} for cases 1, 2, 3, and 4, respectively. Note that the reference area is the total irradiated area, i.e. the area of the irradiation collection, which equals the photoabsorber area if no irradiation concentration is used, or the area of the concentrator if irradiation concentration is used. Given that the semiconductors are often costly components of the device, the total amount of produced hydrogen can also be reported by semiconductor-area, useful for a techno-economic comparison. Hence, the values become 57.1, 3240, 58, and 6010 kg m_{sc}^{-2} for cases 1, 2, 3 and 4. Hence, Case 4, which uses radiation concentration and current dilution, appears to be the most competitive solution. In a case where the electrocatalyst is the most expensive component, the total amount of produced hydrogen reported per electrocatalyst-area is 57.1, 3240, 580, and 601 kg m_{EC}^{-2} for cases 1, 2, 3, and 4. Therefore, Case 2, which uses radiation concentration and no current dilution, appears to be the most competitive solution.

4.2.3. Impact of the design point on performance loss. The cumulated amount of produced hydrogen highly depends on device operating point at the beginning of life. The closer the initial operating point is to the maximal power point of the photoabsorber, the more dramatic the impact of degradation on performance (even starting within the initial operating hours). However, the farther the operating point is from the maximum power point (at potentials smaller than the V_{oc}), the larger the overdesign of the photoabsorber, leading to an extra expense for a large V_{oc} photoabsorber. Thus, a tradeoff between photoabsorber overdesign and durability is found. We use Case 4 (introduced in section 4.2.2) to compare two

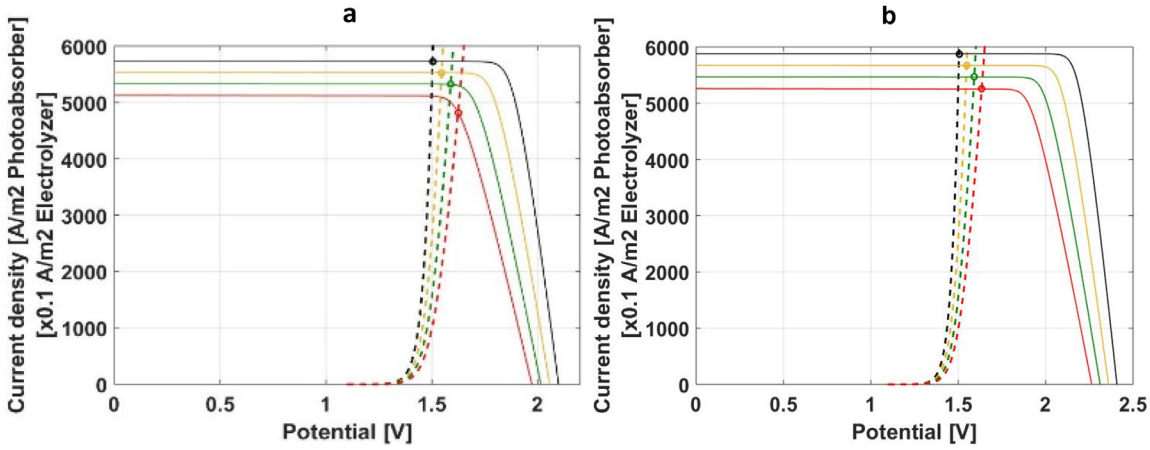

Figure 6. Evolutions of the *i–V* curves during the first 30 000 operating hours of a device with radiation concentration ($C = 100$) and current dilution ($F = 10$). (a) Semiconductor with $i_{sc,0} = 191$ A m^{-2} and $V_{oc} = 2.01$ V. (b) Semiconductor $i_{sc,0} = 196$ A m^{-2} and $V_{oc} = 2.32$ V. The black, yellow, green, and red lines correspond to 0, 10 000, 20 000, and 30 000 h. The circles indicate the operating points at different times.

different semiconductors with different V_{oc}, but very similar i_{sc}: SC 2 ($i_{sc,0} = 191$ A m^{-2}, $V_{oc} = 2.01$ V) and SC 3 ($i_{sc,0} = 196$ A m^{-2}, $V_{oc} = 2.32$ V). The obtained evolutions of the current density versus voltage curves, using both semiconductors at the yearly mean operating radiation flux (300 W m^{-2}), are presented in figure 6.

We observe that good durability can be obtained if the design point of the device is far from the maximum power point of the photoabsorber (using the SC 3). For comparison, the total amount of produced hydrogen moves from 60.1 to 62.3 kg m^{-2} (per concentrator collection area) when a photoabsorber with a higher open circuit voltage is used. If the operating point remains in the 'plateau' region, decreases in the hydrogen production rate mainly depend on the degradation of the photocurrent and shunt resistance of the photoabsorber. Because of this, solar cells with high open circuit voltages and low series resistances should be used, but this increases the cost.

5. Summary and conclusion

We reviewed degradations of integrated photoelectrochemical (PEC) devices and developed a case study to illustrate their impact on evolutions in performance.

First, we identified and discussed the relevance of integrating investigations of durability into the design of photoelectrochemical devices, and we defined lifetime targets for economically competitive and sustainable PEC device approaches. An overview of all reported long-term PEC operating studies and associated device lifetimes was given, and the main challenges were summarized. We presented the different components required for the functionality of a PEC device (semiconductor, catalyst, and solid and liquid electrolyte), and discussed the interfaces present in different PEC device configurations. Degradations of the individual components were described in detail, and the parameters influencing them were presented.

For the semiconductor, degradation mechanisms reviewed include: chemical corrosion, electrochemical corrosion, photoelectrochemical corrosion, chemical destabilization, protonation, and hydroxylation. For the electrocatalyst, the presented degradation mechanisms include: dissolution, agglomeration, deactivation, and catalyst support corrosion. For solid electrolytes, we dicussed: chemical attack, poisoning by foreign ions, mechanical degradation, phototendering, photolysis, and embrittlement. For the liquid electrolyte, degradation mechanisms reviewed include: pollution, salt deposits, and saturation. We further discussed how the individual component degradation affects integrated device degradation, as well as how device design and operation affects component degradation. The degradation of three different PEC device designs and four different operating conditions were estimated in detail using a simplified *bottom-up* modeling approach. Different degradation rates of device components (reported in literature) were used to predict degradation in the performance and durability of PEC devices. We highlighted how PEC device design choice and applied operating conditions boost the salience of various degradation mechanisms, and how these impact the overall device lifetime.

We find that the semiconductor-liquid electrolyte junction is the most challenging interface for short-term stability, while catalyst and electrolyte degradation is more relevant and challenging for reliability and long term durability. We also find that different degradation mechanisms are relevant for different device designs. In particular, exposing the photoabsorber directly to the electrolyte, or protecting it (using protecting films or separation through wires), significantly affects the degradation of photoabsorber components. Similarly, exposing electrocatalysts directly to irradiation or hiding them in the dark significantly affects degradation of the catalysts. For PEC device designs utilizing wires and separating charge generation (i.e. photoabsorbers) and electrochemical reaction (i.e. catalysts), the risk of self-oxidization of the semiconductor instead of the reactant (i.e. water) is eliminated, and long-term durability is more plausible. Monolithic designs, on the other hand, require the use of liquid electrolytes, which are often strongly acidic or basic, in order to reduce the solution conductivity losses and pH gradient overpotentials, with the negative effect of a dramatic enhancement in photocorrosion.

There are various promising solutions to increase the durability of PEC devices utilizing catalyst-decorated photoabsorbers directly immersed in liquid electrolyte, such as: (i) the discovery and testing of new semiconductors which are stable in strongly acidic/basic electrolytes, or (ii) the development of new materials and new techniques to protect unstable semiconductors.

The case study presented here provides a simple *bottom-up* macroscopic modeling tool to assess the impact of component integration and combination, component degradation, and device design and operation on long-term integrated device performance and durability. As inputs, we used degradation rates of the various components cited in literature. Our tools can provide quantification of device degradation, and guide the choice of components, device design, and device operating conditions. Our modeling results predict that the cumulative amount of produced hydrogen during the lifetime of a device highly depends on device design choice, on irradiation intensity and concentration as well as on the current density and concentration in the design, and on the initial design operating point of the device. The initial design operating point of the PEC device must consider the tradeoff between the expense of a high-voltage photoabsorber and performance loss with aging. The closer the initial design point to the maximum power point of the photoabsorber, the more dramatic the performance degradation, even during the first hours.

Globally, to mitigate degradation of PEC devices, different reference scales should be considered simultaneously. At the scale of components, new materials as well as new deposition and coating techniques should be developed. At the scale of the cell, component integration and device design should be optimized. An appropriate component integration should limit the occurrence of non-stable interfaces (depending on the materials of the components) and the exposure of components prone to photo-driven degradation processes under irradiation (see figure 2). Once the particular integration is chosen, the design of the cell (positions, dimensions, and orientations) should simultaneously optimize the position of the initial operating point (with respect to the maximum power point of the photoabsorber), and limit current density heterogeneities while avoiding local hot spots. At the system scale, appropriate prognostics and heath management of the PEC device should be performed in order to identify degradation sources. In this manner, the heat and water management, device maintenance, and component replacement can be optimized.

Future degradation investigations should focus on the understanding, characterization, and quantification of the effect of each degradation mechanism on the physical properties of components, and examine how durability and reliability testing can be used to trace the source of degradation mechanisms. Furthermore, atomistic-scale degradation models studying the kinetics of degradation mechanisms should be coupled to continuum-scale device performance models in order to predict evolution of the efficiency and purity of produced hydrogen, and to prevent catastrophic device failure. In parallel, PEC devices should be developed and tested under real operating conditions, with appropriate durability testing protocols. Appropriate accelerated stress tests, taking into account all of the real time transients of devices should be defined. Moreover, reference testing conditions should be introduced for benchmarking of degradation studies and reasonable lifetimes and durability targets should be defined. Simultaneous combination of experimental and numerical results will improve the development of efficient, low cost, sustainable, and durable photoelectrochemical devices and provide a pathway for the practical large-scale implementation of PEC-based solar hydrogen processing plants.

Acknowledgments

This material is based upon work performed with the financial support of the Nano-Tera.ch initiative as part of the SHINE project (Grant #145936), and the Starting Grant of the Swiss National Science Foundation as part of the SCOUTS project (Grant #155876). We thank Sarah Robinson for careful editing.

References

[1] Dumortier M, Tembhurne S and Haussener S 2015 *Energy Environ. Sci.* **8** 3614–28
[2] Bockris J O 1972 *Science* **176** 1323
[3] Barreto L, Makihira A and Riahi K 2003 *Int. J. Hydrog. Energy* **28** 267–84
[4] Muradov N Z and Veziroglu T N 2005 *Int. J. Hydrog. Energy* **30** 225–37
[5] Lewis N S 2007 *MRS Bull.* **32** 808–20
[6] Tributsch H 2008 *Int. J. Hydrog. Energy* **33** 5911–30
[7] Haussener S, Hu S, Xiang C, Weber A Z and Lewis N 2013 *Energy Environ. Sci.* **6** 3605–18
[8] Khaselev O and Turner J A 1998 *Science* **280** 425–7
[9] Licht S, Wang B and Mukerji S 2000 *J. Phys. Chem.* B **104** 8920–4
[10] Peharz G, Dimroth F and Wittstadt U 2007 *Int. J. Hydrog. Energy* **32** 3248–52
[11] Abdi F F, Han L, Smets A H, Zeman M, Dam B and van de Krol R 2013 *Nat. Commun.* **4** 1–7
[12] Luo J, Im J H, Mayer M T, Schreier M, Nazeeruddin M K, Park N G, Tilley S D, Fan H J and Grätzel M 2014 *Science* **345** 1593–6
[13] Han L, Abdi F F, Van de Krol R, Liu R, Huang Z, Lewerenz H J, Dam B, Zeman M and Smets A H M 2014 *ChemSusChem* **7** 2832–8
[14] James B D, Baum G N, Perez J and Baum K N 2009 Technoeconomic analysis of photoelectrochemical (pec) hydrogen production *Technical Report* Directed Technologies Inc
[15] Pinaud B A *et al* 2013 *Energy Environ. Sci.* **6** 1983–2002
[16] Rodriguez C A, Modestino M A, Psaltis D and Moser C 2014 *Energy Environ. Sci.* **7** 3828–35
[17] Kirner S, Bogdanoff P, Stannowski B, van de Krol R, Rech B and Schlatmann R 2016 *Int. J. Hydrog. Energy* **41** 20823–31
[18] Zhai P, Haussener S, Ager J, Sathre R, Walczak K, Greenblatt J and McKone T 2013 *Energy Environ. Sci.* **6** 2380–9
[19] Sathre R, Scown C D, Morrow W R, Stevens J C, Sharp I D, Ager J W, Walczak K, Houle F A and Greenblatt J B 2014 *Energy Environ. Sci.* **7** 3264–78

[20] Sathre R, Greenblatt J B, Walczak K, Sharp I D, Stevens J C, Ager J W and Houle F A 2016 *Energy Environ. Sci.* **9** 803–819
[21] Ager J W, Shaner M R, Walczak K A, Sharp I D and Ardo S 2015 *Energy Environ. Sci.* **8** 2811–24
[22] Doscher H, Young J L, Geisz J F, Turner J A and Deutsch T G 2016 *Energy Environ. Sci.* **9** 74–80
[23] Chen Z *et al* 2010 *J. Mater. Res.* **25** 3–16
[24] International Energy Agency 2014 Technology roadmap, solar photovoltaic energy *Technical Report*
[25] Bertuccioli L 2014 Development of water electrolysis in the European union *Technical Report* E4tech, Element Energy
[26] Barbir F 2005 *Solar Energy* **78** 661–669
[27] Bloom I, Walker L K, Basco J K, Malkow T, Saturnio A, Marco G D and Tsotridis G 2013 *J. Power Sources* **243** 451–7
[28] Mukundan R *et al* 2013 Accelerated testing validation *Technical Report* LANL
[29] Petrone R, Hissel D, Pera M, Chamagne D and Gouriveau R 2015 *Int. J. Hydrog. Energy* **40** 12489–505
[30] Anderson E 2016 PEM electrolyzer reliability based on 20 years of product experience in commercial markets *2nd Int. Workshop on Durability and Degradation Issues in PEM Electrolysis Cells and its Components*
[31] Shi Z, Wen X, Guan Z, Cao D, Luo W and Zou Z 2015 *Ann. Phys.* **358** 236–47
[32] Hu S, Lewis N S, Ager J W, Yang J, McKone J R and Strandwitz N C 2015 *J. Phys. Chem.* C **119** 24201–28
[33] Chen Y, Feng X, Liu M, Su J and Shen S 2016 *Nanophotonics* **5** 524–547
[34] Yamada Y, Matsuki N, Ohmori T, Mametsuka H, Kondo M, Matsuda A and Suzuki E 2003 *Int. J. Hydrog. Energy* **28** 1167–9
[35] Kainthla R C, Zelenay B and Bockris J O 1986 *J. Electrochem. Soc.* **133** 248–53
[36] Sun K, McDowell M T, Nielander A C, Hu S, Shaner M R, Yang F, Brunschwig B S and Lewis N S 2015 *J. Phys. Chem. Lett.* **6** 592–8
[37] Urbain F, Smirnov V, Becker J P, Lambertz A, Rau U and Finger F 2016 *Solar Energy Mater. Solar Cells* **145** 142–7
[38] Kelly N A and Gibson T L 2006 *Int. J. Hydrog. Energy* **31** 1658–73
[39] Zhang L, Minegishi T, Nakabayashi M, Suzuki Y, Seki K, Shibata N, Kubota J and Domen K 2015 *Chem. Sci.* **6** 894–901
[40] Young J L, Steirer K X, Dzara M J, Turner J A and Deutsch T G 2016 *J. Mater. Chem.* A **4** 2831–6
[41] Verlage E, Hu S, Liu R, Jones R J R, Sun K, Xiang C, Lewis N S and Atwater H A 2015 *Energy Environ. Sci.* **8** 3166–72
[42] Shaner M R, Hu S, Sun K and Lewis N S 2015 *Energy Environ. Sci.* **8** 203–7
[43] Tamirat A G, Rick J, Dubale A A, Su W N and Hwang B J 2016 *Nanoscale Horiz.* **1** 243–67
[44] Xu P, Feng J, Fang T, Zhao X, Li Z and Zou Z 2016 *RSC Adv.* **6** 9905–10
[45] Lopes T, Dias P, Andrade L and Mendes A 2014 *Sol. Energy Mater. Sol. Cells* **128** 399–410
[46] Carmo M, Fritz D L, Mergel J and Stolten D 2013 *Int. J. Hydrog. Energy* **38** 4901–34
[47] Fouda-Onana F, Chandesris M, Médeau V, Chelghoum S, Thoby D and Guillet N 2016 *Int. J. Hydrog. Energy* **41** 16627–36
[48] Nandjou F, Poirot-Crouvezier J P, Chandesris M, Blachot J F, Bonnaud C and Bultel Y 2016 *J. Power Sources* **326** 182–92
[49] Ronge J, Nijs D, Kerkhofs S, Masschaele K and Martens J A 2013 *Phys.Chem. Chem. Phys.* **15** 315–9325
[50] Dumortier M, Bosserez T, Rongé J, Martens J and Haussener S 2016 *J. Phys. Chem.* C **120** 3705–14
[51] Lewerenz H J 2014 *J. Electrochem. Soc.* **161** H3117–29
[52] Bergen A, Pitt L, Rowe A, Wild P and Djilali N 2009 *Int. J. Hydrog. Energy* **34** 64–70
[53] Ursúa A, Martín I S, Barrios E L and Sanchis P 2013 *Int. J. Hydrog. Energy* **38** 14952–67
[54] Ursúa A, Barrios E L, Pascual J, Martin I S and Sanchis P 2016 *Int. J. Hydrog. Energy* **41** 12852–61
[55] Dubau L *et al* 2014 *Wiley Interdiscip. Rev. Energy Environ.* **3** 540–560
[56] Chatillon Y, Bonnet C and Lapicque F 2014 *Fuel Cells* **4** 581–9
[57] Grätzel M 2001 *Nature* **414** 338–44
[58] Chen S and Wang L W 2012 *Chem. Mater.* **24** 3659–66
[59] Bak T, Nowotny J, Rekas M and Sorrell C 2002 *Int. J. Hydrog. Energy* **27** 991–1022
[60] Linkous C, Anderson H, Kopitzke R and Nelson G 1998 *Int. J. Hydrog. Energy* **23** 525–9
[61] Jang I Y, Kweon O H, Kim K E, Hwang G J, Moon S B and Kang A S 2008 *J. Membr. Sci.* **322** 154–161
[62] Wei G, Xu L, Huang C and Wang Y 2010 *Int. J. Hydrog. Energy* **35** 7778–83
[63] Rikukawa M and Sanui K 2000 *Prog. Polym. Sci.* **25** 1463–502
[64] Antonucci V, Blasi A D, Baglio V, Ornelas R, Matteucci F, Ledesma-Garcia J, Arriaga L and Aricò A 2008 *Electrochim. Acta* **53** 7350–6
[65] Baglio V, Ornelas R, Matteucci F, Martina F, Ciccarella G, Zama I, Arriaga L, Antonucci V and Aricò A S 2009 *Fuel Cells* **3** 247–52
[66] Albert A, Barnett A O, Thomassen M S, Schmidt T J and Gubler L 2015 *ACS Appl. Mater. Interfaces* **7** 22203–12
[67] Albert A, Lochner T, Schmidt T J and Gubler L 2016 *ACS Appl. Mater. Interfaces* **8** 15297–306
[68] Mauritz K A and Moore R B 2004 *Chem. Rev.* **104** 4535–86
[69] Zeng K and Zhang D 2010 *Prog. Energy Combust. Sci.* **36** 307–26
[70] Aili D, Hansen M K, Andreasen J W, Zhang J, Jensen J O, Bjerrum N J and Li Q 2015 *J. Membr. Sci.* **493** 589–98
[71] Rosa M, Santos F and Silva P D 1995 *Int. J. Hydrog. Energy* **9** 697–700
[72] Otero J, Sese J, Michaus I, Maria M S, Guelbenzu E, Irusta S, Carrilero I and Arruebo M 2014 *J. Power Sources* **247** 967–74
[73] Ohmori T, Tachikawa K, Tsuji K and Anzai K 2007 *Int. J. Hydrog. Energy* **32** 5094–7
[74] Ayers K E, Anderson E B, Capuano C B, Carter B D, Dalton L T, Hanlon G, Manco J and Niedzwiecki M 2010 *ECS Trans.* **33** 3–15
[75] Walter M G, Warren E L, McKone J R, Boettcher S W, Mi Q, Santori E A and Lewis N S 2010 *Chem. Rev.* **110** 6446–73
[76] Rasten E, Hagen G and Tunold R 2003 *Electrochim. Acta* **48** 3945–52
[77] Millet P, Ngameni R, Grigoriev S, Mbemba N, Brisset F, Ranjbari A and Etiévant C 2010 *Int. J. Hydrog. Energy* **35** 5043–52
[78] Haussener S, Xiang C, Spurgeon J M, Ardo S, Lewis N S and Weber A Z 2012 *Energy Environ. Sci.* **5** 9922–35
[79] Walczak K *et al* 2015 *ChemSusChem* **8** 544–51
[80] Jacobsson T J, Fjallstrom V, Edoff M and Edvinsson T 2014 *Energy Environ. Sci.* **7** 2056–70
[81] Modestino M A and Haussener S 2015 *Ann. Rev. Chem. Biomol. Eng.* **6** 13–34
[82] Bosserez T, Rongé J, van Humbeeck J, Haussener S and Martens J 2015 *IFP Energies Nouvelles Int. Conf.*
[83] Chen Y, Xiang C, Hu S and Lewis N S 2014 *J. Electrochem. Soc.* **161** F1101–10
[84] Newman J 2013 *J. Electrochem. Soc.* **160** F309–11
[85] Urbain F *et al* 2015 *Chem. Phys. Lett.* **638** 25–30

[86] Fujishima A and Honda K 1972 *Nature* **238** 37–8
[87] Tembhurne S and Haussener S 2016 *J. Electrochem. Soc.* **163** H988–98
[88] Devabhaktuni V, Alam M, Depuru S S S R, Green R C II, Nims D and Near C 2013 *Renew. Sustain. Energy Rev.* **19** 555–64
[89] Anderson E, Ayers K and Capuano C 2013 R&D focus areas based on 60'000 hr life PEM water electrolysis stack experience *First Int. Workshop on Durability and Degradation Issues in PEM Electrolysis Cells and its Components*
[90] Young J L, Döscher H, Turner J A, and Deutsch T G 2016 *J. Phys. Chem.* C **120** 4418–22
[91] Pourbaix M 1974 *Atlas of Electrochemical Equilibria in Aqueous Solutions* (Houston, TX: National Association of Corrosion Engineers)
[92] Allongue P, Costa-Kieling V and Gerischer H 1993 *J. Electrochem. Soc.* **140** 1009–18
[93] Glembocki O J, Stahlbush R E and Tomkiewicz M 1985 *J. Electrochem. Soc.* **132** 145–51
[94] Nikolaychuk P A 2014 *Silicon* **6** 109–116
[95] Krol R V D and Grätzel M 2012 *Photoelectrochemical Hydrogen Production* (New York: Springer)
[96] Caccamo L *et al* 2016 *ACS Appl. Mater. Interfaces* **8** 8232–8
[97] Greischer H, Kautec W, Decker F, Scholz G A, Ross D, Lubke M and Wasle S 1984 *Report* EUR 9531 EN Commission of the European Communities
[98] Zhou L *et al* 2016 *Phys. Chem. Chem. Phys.* **18** 9349–52
[99] Aguiar J A, Anderson N C and Neale N R 2016 *J. Mater. Chem.* A **4** 8123–9
[100] Lai J, Yuan D, Huang P, Zhang J, Su J J, Tian Z W and Zhan D 2016 *J. Phys. Chem.* C **120** 16446–52
[101] Mei B, Seger B, Pedersen T, Malizia M, Hansen O, Chorkendorff I and Vesborg P C K 2014 *J. Phys. Chem. Lett.* **5** 1948–52
[102] Hu S, Shaner M R, Beardslee J A, Lichterman M, Brunschwig B S and Lewis N S 2014 *Science* **344** 1005–9
[103] Mei B, Pedersen T, Malacrida P, Bae D, Frydendal R, Hansen O, Vesborg P C K, Seger B and Chorkendorff I 2015 *J. Phys. Chem.* C **119** 5019–15027
[104] Didden A, Hillebrand P, Dam B and van de Krol R 2015 *Int. J. Photoenergy* **2015** 1–8
[105] Avrami M 1940 *J. Chem. Phys.* **8** 212–24
[106] Lichterman M F *et al* 2016 *Catalysis Today* **262** 11–23
[107] Cox C R, Winkler M T, Pijpers J J H, Buonassisi T and Nocera D G 2013 *Energy Environ. Sci.* **6** 532–538
[108] Mirletz H M, Peterson K A, Martin I T and French R H 2015 *Sol. Energy Mater. Sol. Cells* **143** 529–38
[109] Sun K *et al* 2015 *Proc. Natl Acad. Sci.* **112** 3612–7
[110] Sun K, Kuang Y, Verlage E, Brunschwig B S, Tu C W and Lewis N S 2015 *Adv. Energy Mater.* **5** 1–8
[111] Scheuermann A G and McIntyre P C 2016 *J. Phys. Chem. Lett.* **7** 2867–78
[112] Rovelli L, Tilley S D and Sivula K 2013 *ACS Appl. Mater. Interfaces* **5** 8018–24
[113] Esposito D V *et al* 2015 *Energy Environ. Sci.* **8** 2863–85
[114] Toma F M *et al* 2016 *Nat. Commun.* **7** 1–11
[115] Halverson A F, Zhu K, Erslev P T, Kim J Y, Neale N R, and Frank A J 2012 *Nano Lett.* **12** 2112–6
[116] Calero S J, Ortiz P, Onate A F and Cortés M T 2016 *Int. J. Hydrog. Energy* **41** 4922–30
[117] Reichman B and Bard A J 1979 *J. Electrochem. Soc.* **126** 583–91
[118] Tamura H, Mita K, Tanaka A and Ito M 2001 *J. Colloid Interface Sci.* **243** 202–7
[119] Li J and Wu N 2015 *Catal. Sci. Technol.* **5** 1360–84
[120] Weng B, Yang M Q, Zhang N and Xu Y J 2014 *J. Mater. Chem.* A **2** 9380–9
[121] Wu L, Zhang Y, Li X and Cen C 2014 *Phys. Chem. Chem. Phys.* **16** 15339–45
[122] Zhang Y, Zhang J, Nie M, Sun K, Li C and Yu J 2015 *J. Nanopart. Res.* **17** 1–11
[123] Kim T W and Choi K S 2016 *J. Phys. Chem. Lett.* **7** 447–51
[124] Han C, Yang M Q, Weng B and Xu Y J 2014 *Phys. Chem. Chem. Phys.* **16** 16891–903
[125] Doering R 2007 *Handbook of Semiconductor Manufacturing Technology* (Boca Raton, FL: CRC Press)
[126] Ndiaye A, Charki A, Kobi A, Kébé C M, Ndiaye P A and Sambou V 2013 *Sol. Energy* **96** 140–51
[127] Perez-Quintana I, Martel A and Hernandez L 2001 *Solid-State Electron.* **45** 2017–21
[128] Schneller E J *et al* 2016 *Renew. Sustain. Energy Rev.* **59** 992–1016
[129] Nehme B, M'Sirdi N K, Akiki T and Naamane A 2014 *Energy Proc.* **62** 565–75
[130] Blish R and Durrant N 2000 Semiconductor device reliability failure models *Technical Report* International SEMATECH
[131] Hacke P, Spataru S, Terwilliger K, Perrin G, Glick S, Kurtz S and Wohlgemuth J 2015 *IEEE J. Photovolt.* **5** 1549–53
[132] Peck S 1986 *Reliability Physics Symp.* pp 44–50
[133] Gimenez S and Bisquert J 2016 *Photoelectrochemical Solar Fuel Production* (Cham: Springer)
[134] McCrory C C L, Jung S, Peters J C and Jaramillo T F 2013 *J. Am. Chem. Soc.* **135** 16977–87
[135] McCrory C C L, Jung S, Ferrer I M, Chatman S M, Peters J C and Jaramillo T F 2015 *J. Am. Chem. Soc.* **137** 4347–57
[136] Cherevko S, Reier T, Zeradjanin A R, Pawolek Z, Strasser P and Mayrhofer K J 2014 *Electrochem. Commun.* **48** 81–5
[137] Brightman E, Dodwell J, van Dijk N and Hinds G 2015 *Electrochem. Commun.* **52** 1–4
[138] Audichon T, Mayousse E, Napporn T W, Morais C, Comminges C and Kokoh K B 2014 *Electrochim. Acta* **132** 284–291
[139] Rakousky C, Reimer U, Wippermann K, Carmo M, Lueke W and Stolten D 2016 *J. Power Sources* **326** 120–128
[140] Borup R L, Davey J R, Garzon F H, Wood D L and Inbody M A 2006 *J. Power Sources* **163** 76–81
[141] Shao-Horn Y, Sheng W C, Chen S, Ferreira P J, Holby E F and Morgan D 2007 *Top. Catalysis* **46** 285–305
[142] Okada T, Ayato Y, Dale J, Yuasa M, Sekine I and Asbjornsen O A 2000 *Phys. Chem. Chem. Phys.* **2** 3255–61
[143] Sun S, Shao Z, Yu H, Li G and Yi B 2014 *J. Power Sources* **267** 515–20
[144] Wei G, Wang Y, Huang C, Gao Q, Wang Z and Xu L 2010 *Int. J. Hydrog. Energy* **35** 3951–7
[145] Todd G and Deutsch J A T 2014 Semiconductor materials for photoelectrolysis *U.S. DOE Hydrogen & Fuel Cells Program Review*
[146] Yano H, Watanabe M, Iiyama A and Uchida H 2016 *Nano Energy* accepted
[147] Li X, Yu J, Low J, Fang Y, Xiao J and Chen X 2015 *J. Mater. Chem.* A **3** 2485–34
[148] Li Y, Xu H, Zhao H, Lu L and Sun X 2016 *J. Appl. Electrochem.* **46** 183–9
[149] Li J, Wang K, Yang Y, McDermid S and Kundu S 2014 Additives to mitigate catalyst layer degradation in fuel cells *US Patent* US8758955 B2
[150] Yang C, Zhou M, Zhang M and Gao L 2016 *Electrochim. Acta* **188** 529–36
[151] Zhou Y, Pasquarelli R, Holme T, Berry J, Ginley D and O'Hayre R 2009 *J. Mater. Chem.* **19** 7830–8
[152] Osgood H, Devaguptapu S V, Xu H, Cho J and Wu G 2016 *Nano Today* **11** 601–25

[153] Sapountzi F M, Gracia J M, Weststrate C K J, Fredriksson H O and Niemantsverdriet J H 2017 *Prog. Energy Combust. Sci.* **58** 1–35
[154] Du L, Shao Y, Sun J, Yin G, Liu J and Wang Y 2016 *Nano Energy* accepted
[155] Rozain C, Mayousse E, Guillet N and Millet P 2016 *Appl. Catalysis* B **182** 123–31
[156] Lettenmeier P *et al* 2016 *Electrochim. Acta* **210** 502–11
[157] Santos D M F, Sequeiral C A C and Figueiredo J L 2013 *Quim. Nova* **36** 1176–93
[158] Krstajic N, Popovic M, Grgur B, Vojnovic M and Sepa D 2001 *J. Electroanal. Chem.* **512** 27–35
[159] Vermeiren P, Adriansens W, Moreels J and Leysen R 1998 *Int. J. Hydrog. Energy* **23** 321–4
[160] Chandesris M, Médeau V, Guillet N, Chelghoum S, Thoby D and Fouda-Onana F 2015 *Int. J. Hydrog. Energy* **40** 1353–66
[161] Wong K H and Kjeang E 2015 *ChemSusChem* **8** 1072–82
[162] Fenton H J H 1894 *J. Chem. Soc. Trans.* **65** 899–910
[163] Petrina S A 2013 Water soprtion, viscoelastic, and optical properties of thin Nafion films *Master's Thesis* Pennsylvania State University, State College, PA
[164] Fox E, Greenway S and Clark E 2009 Radiation stability of nafion membranes used for isotope separation by proton exchange membrane electrolysis *Technical Report* Savannah River National Laboratory
[165] Wang X, Zhang L, Li G, Zhang G, Shao Z G and Yi B 2015 *Electrochim. Acta* **158** 253–7
[166] Okada T, Moller-Holst S, Gorseth O and Kjelstrup S 1998 *J. Electroanal. Chem.* **442** 137–45
[167] Grigoriev S, Dzhus K, Bessarabov D and Millet P 2014 *Int. J. Hydrog. Energy* **39** 20440–6
[168] Rozain C and Millet P 2014 *Electrochim. Acta* **131** 160–7
[169] Zamel N 2013 Approaches and methodology on accelerated stress tests in fuel cells *1st Int. Workshop on Durability and Degradation Issues in PEM Electrolysis Cells and its Components*
[170] Iwai Y, Hiroki A, Tamada M and Yamanishi T 2008 *J. Membr. Sci.* **322** 249–55
[171] Conti F, Negro E and Noto V D 2009 *ChemComm* 7006–8
[172] Wu J, Yuan X Z, Martin J J, Wang H, Zhang J, Shen J, Wu S and Merida W 2008 *J. Power Sources* **184** 104–119
[173] Liu F, Yi B, Xing D, Yu J and Zhang H 2003 *J. Membr. Sci.* **212** 213–23
[174] Weissbach T, Peckham T J and Holdcroft S 2016 *J. Membr. Sci.* **498** 94–104
[175] Sethuraman V A, Weidner J W, Haug A T, Motupally S and Protsailo L V 2008 *J. Electrochem. Soc.* **155** B50–7
[176] Lettenmeier P, Wang R, Abouatallah R, Burggraf F, Gago A S and Friedrich K A 2016 *J. Electrochem. Soc.* **163** F3119–24
[177] Gago A *et al* 2016 *J. Power Sources* **307** 815–25
[178] Jung H Y, Huang S Y and Popov B N 2010 *J. Power Sources* **195** 1950–6
[179] Kuromoto N K, Simao R A and Soares G A 2007 *Mater. Charact.* **58** 114–21
[180] Wang C C 2013 Corrosion resistant metallic components for electrochemical devices *1st Int. Workshop Durability and Degradation Issues in PEM Electrolysis Cells and Its Components*
[181] Park J, Oh H, Ha T, Lee Y I and Min K 2015 *Appl. Energy* **155** 866–80
[182] Mo J, Steen S M III, Zhang F Y, Toops T J, Brady M P and Green J B Jr 2015 *Int. J. Hydrog. Energy* **40** 12506–11
[183] Mo J, Kang Z, Yang G, Retterer S T, Cullen D A, Toops T J, Green J B Jr and Zhang F Y 2016 *Appl. Energy* **177** 817–22
[184] Dhanushkodi S, Capitanio F, Biggs T and Merida W 2015 *Int. J. Hydrog. Energy* **40** 16846–59
[185] Lapicque F, Belhadj M, Bonnet C, Pauchet J and Thomas Y 2016 *J. Power Sources* **336** 40–53
[186] Han B, Mo J, Kang Z and Zhang F Y 2016 *Electrochim. Acta* **188** 317–26
[187] Lee C, Hinebaugh J, Banerjee R, Chevalier S, Abouatallah R, Wang R and Bazylak A 2016 *Int. J. Hydrog. Energy* accepted
[188] Robin C, Gerard M, Franco A A and Schott P 2013 *Int. J. Hydrog. Energy* **38** 4675–88
[189] Zhang X and Bieberle-Hutter A 2016 *ChemSusChem* **9** 1223–42
[190] Phinikarides A, Kindyni N, Makrides G and Georghiou G E 2014 *Renew. Sustain. Energy Rev.* **40** 143–52
[191] Mench M M, Kumbur E C and Veziroglu T N 2012 *Polymer Electrolyte Fuel Cell Degradation* (Cambridge, MA: Academic)
[192] Tembhurne S and Haussener S 2016 *J. Electrochem. Soc.* **163** H999–1007
[193] Fouda-Onana F 2016 AST protocols for PEM water electrolysis: insight on performances and components degradation *2nd Int. Workshop on Durabiltiy and Degradation Issues in PEM Electrolysis cells and its Components*
[194] Garcia-Valverde R, Espinosa N and Urbina A 2011 *Int. J. Hydrog. Energy* **36** 10574–86
[195] Junsangsri P and Lombardi F 2010 *25th Int. Symp. on Defect and Fault Tolerance in VLSI Systems*
[196] Nualhong D 2016 *Assessing Degradation of Solar Cells Using Single Diode Model* (Nonthaburi: Electricity Generating Authority of Thailand)
[197] Weicht J A, Hamelmann F U and Behrens G 2014 Parameter variation of the one-diode model of a-Si and a-Si/μc-Si solar cells for modeling light-induced degradation *J. Phys.: Conf. Ser.* **559** 012017
[198] Weicht J A, Hamelmann F U and Behrens G 2016 Simulation of light-induced degradation of μc-Si in a-Si/μc-Si tandem solar cells by the diode equivalent circuit *J. Phys.: Conf. Ser.* **682** 012017
[199] Friesen T 2015 Lifetime degradation mechanisms *Technical Report* PERFPLUS
[200] Kaplanis S and Kaplani E 2011 *Simul. Modelling Pract. Theory* **19** 1201–11
[201] Park N, Jeong J and Han C 2014 *Microelectron. Reliab.* **54** 1562–66
[202] Shockley W and Queisser H J 1961 *J. Appl. Phys.* **32** 510–9